iScience

CellPress
OPEN ACCESS

Article

Low frequency independent components: Internal neuromarkers linking cortical LFPs to behavior

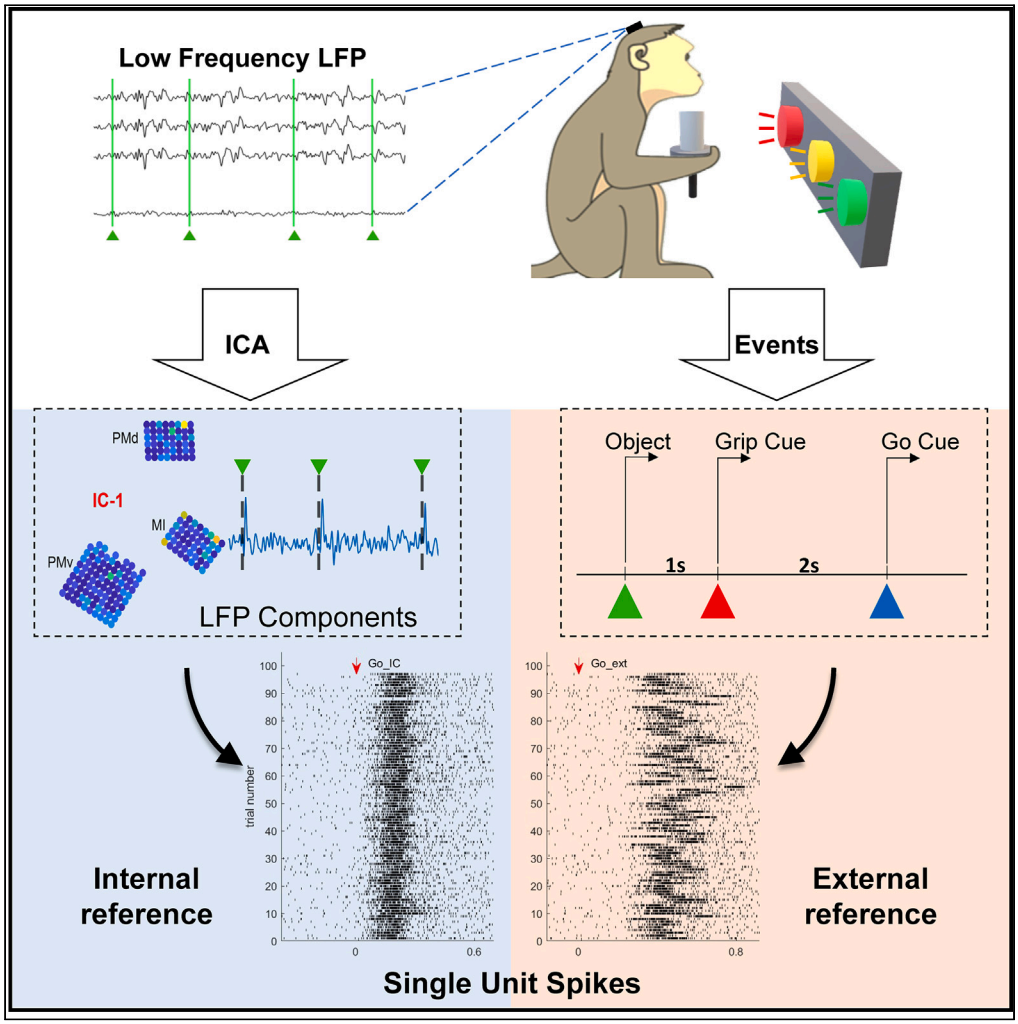

Diego Orellana V., John P. Donoghue, Carlos E. Vargas-Irwin

carlos_vargas_irwin@brown.edu

Highlights

LFP ICs display peaks associated with behavioral task events

LFP ICs improve spike alignment and task stage detection

Components maintain high spatial and temporal consistency across recording sessions

Specific components potentially represent transitions between cortical network states

Orellana V. et al., iScience 27, 108310
February 16, 2024
https://doi.org/10.1016/j.isci.2023.108310

iScience

CellPress
OPEN ACCESS

Article

Low frequency independent components: Internal neuromarkers linking cortical LFPs to behavior

Diego Orellana V.,[4,5] John P. Donoghue,[1,2,3] and Carlos E. Vargas-Irwin[1,2,3,6,*]

SUMMARY

Local field potentials (LFPs) in the primate motor cortex have been shown to reflect information related to volitional movements. However, LFPs are composite signals that receive contributions from multiple neural sources, producing a complex mix of component signals. Using a blind source separation approach, we examined the components of neural activity recorded using multielectrode arrays in motor areas of macaque monkeys during a grasping and lifting task. We found a set of independent components in the low-frequency LFP with high temporal and spatial consistency associated with each task stage. We observed that ICs often arise from electrodes distributed across multiple cortical areas and provide complementary information to external behavioral markers, specifically in task stage detection and trial alignment. Taken together, our results show that it is possible to separate useful independent components of the LFP associated with specific task-related events, potentially representing internal markers of transition between cortical network states.

INTRODUCTION

The neural processes underlying a wide variety of tasks reside in the coordinated activity of multiple neuronal subpopulations that form a complex system of local circuits and global networks.[1] Electrical activity recorded in the motor cortex provides useful information at various spatial and temporal scales, from individual neurons (spiking activity) to population neuronal activity represented in local field potentials (LFPs). Single unit spiking activity has been successfully used to predict movement kinematics in a variety of contexts, including neuroprosthetic control.[2–6] LFPs have also been shown to contain movement-related information largely overlapping with single unit spiking.[7–10] LFPs are composite signals that receive contributions from multiple neural sources and are believed to reflect the highly dynamic flow of information in the cerebral cortex. Therefore, understanding their characteristics and temporal patterns of their component signals can help uncover mechanisms of information transfer within and between neural networks.[11] So far, the separation of the sources of electrical activity converging in LFPs is an unresolved problem.[12] Discovering which signals compose LFPs, which subregions give rise to them, and what roles they play, could significantly improve our understanding of the underlying neural mechanisms of cortical computation and network function. Previous studies based on Blind Source Separation (BSS) methods have shown promising results, for example, in 2010 Makarov et al., recorded hippocampal neuronal activity using a linear probe covering the entire CA1 region and implemented an independent component model for blind separation of LFP sources. They identified three main local LFP generators whose information content was much higher than in the raw potentials. These generators coincided with axonal terminal fields of local interneuron subtypes and associative fibers from nearby subfields.[13] In 2014 the same research group examined LFPs recorded with a linear array in the lateral geniculate nucleus (LGN) of a monkey (*Macaca mulatta*) trained to perform a visual task. They showed that, regardless of the complexity of the spatial organization of the units and the population, independent component analysis (ICA) allowed the separation of five stable components that allow a reliable readout of activity in specific afferent populations. In this particular case, these components most likely describe synaptic activity elicited by afferent input from different origins, such as the retina, the cortex, the nucleus reticularis or the midbrain. These components could also be used to quantitatively assess global output at different global brain states.[14] More recently, Senzai et al. (2019) used a high-density silicon probe with 64 collinear registration sites and applied a source separation-oriented approach to mouse LFPs to define functional layers in mouse V1 and relate them to classical anatomical layers. ICA produced six independent components (ICs) with depth distribution consistently related to anatomically defined layers across animals.[15]

[1]Department of Neuroscience, Brown University, Providence, RI 02912, USA
[2]Robert J and Nancy D Carney Institute for Brain Science, Providence, RI 02912, USA
[3]Center for Neurorestoration and Neurotechnology, Rehabilitation Research and Development Service, Department of Veterans Affairs Medical Center, Providence, RI 02908, USA
[4]Engineering Faculty, Pontificia Universidad Javeriana, Bogotá 110231, Colombia
[5]Faculty of Energy, Universidad Nacional de Loja, Loja 110101, Ecuador
[6]Lead contact
*Correspondence: carlos_vargas_irwin@brown.edu
https://doi.org/10.1016/j.isci.2023.108310

The spatial resolution of single-point recordings and even collinear multilayer recordings do not allow the study of neuronal activity distributed over the surface of the motor cortex. Using such recordings, it is impossible to know whether field potentials reflect the activity of a single or multiple presynaptic afferent populations distributed on the cortical surface. Multi-electrode arrays (MEAs) provide the opportunity to sample high-resolution spatial profiles of LFPs across several square millimeters of the cortical surface (~4 square mm), providing a viable alternative to overcome some of these limitations. To our knowledge, there have been no studies focused on the separation and source analysis of intracortical LFPs recorded with MEA technology during voluntary motor tasks.

The primary motor cortex (M1), together with the dorsal premotor cortex (PMd) and ventral premotor cortex (PMv), are thought to be involved in important aspects of perceptual cue processing, motor planning, decision making, action selection and movement execution.[7,16–19] M1 has a substantial role in controlling kinematic and dynamic parameters leading to the production of voluntary movements and constitutes the primary node that transmits voluntary motor commands to the spinal cord using means like the density of direct projections to motor neurons or preponderance of movement related neural discharge.[20–22] The dorsal premotor cortex (PMd) is a region where sensory and action-related information converges to guide voluntary arm movement,[23–25] and PMv is thought to be involved in the coordination of motor activities of distal upper limb movements.[26–28] While this suggests distinct roles for this 'troika' it is also clear that they share many aspects of sensorimotor integration (for a discussion see Begliomini et al., 2014[29]). MEA investigation of LFP signals across these areas may provide a useful measure of the integrative and distinct properties for these closely related areas. Thus, for the present study, microelectrode arrays were chronically implanted in MI, PMd, and PMv, for simultaneous assessment of LFPs while monkeys planned and performed a set of skilled reach and grasp actions. We have shown that low-frequency independent components (LF-ICs) derived from multiarea LFP signals are associated with specific phases of the behavioral task. The activation map for these components (i.e., the weights assigned to electrodes in different areas) shows widespread contributions across MI, PMd and PMv during planning stages, while activation tends to be more focused on MI during movement execution. We interpret these components as indicators of changes in mesoscopic cortical processing modes reflecting specific task requirements. Segmenting neural data streams based on these intrinsic signals could facilitate detection and alignment to neural events of interest, with possible applications in basic neurophysiology and applied brain-computer interface development.

RESULTS

Movement stage-dependent LFP features

We trained two macaque monkeys to perform a cued grasping task with an instructed delay (Figure 1E), this approach allowed us to analyze LFPs separately at each phase of movement. Neuronal activity was recorded simultaneously using MEAs chronically implanted in the primary motor (MI, 48 electrodes), dorsal premotor (PMd, 48 electrodes), and ventral premotor (PMv, 96 electrodes) cortex (Figures 1A and 1C). Monkeys were trained to reach, grasp, and lift one of two objects (A or B), each affording two possible grip types, as previously described in Vargas-Irwin et al., 2015,[30] for a total of three possible grasps (one grip is common to both objects). Each object included an identical 10-cm-long, 3.5-cm-diameter cylinder affording a power grip. For Object A, the cylinder was joined to a horizontal disk with a diameter of 7.5 cm and thickness of 0.5 cm, which the monkeys were trained to grasp using a key grip. In Object B, the cylinder was joined to a vertical plate measuring 10 × 7 × 0.5 cm, which the monkeys were trained to grasp using a precision grip. The monkeys grasped the objects in one of the two ways based upon the following conditional associations: a red light indicated a power grasp, and a yellow light indicated a key or precision grasp (depending on which object was present). In each recording session, the monkeys performed between 80 and 150 successfully completed trials. The experimental device was equipped with multiple sensors (see method details) to identify the onset of each task stage. The temporal sequence of seven event markers is shown in Figure 1E. The first marker, "Object," marks the moment when the object was illuminated in an otherwise completely dark room, the second, "Grip Cue," marked the grasp-type cue appearance, the third, "Go Cue," marked the onset of the visual GO instruction. Four subsequent markers corresponded to the execution phase of the task, denoting the initiation of movement "Start" (when the hand was lifted from a contact sensing pad), the beginning of the lift "Lift beg," the end of the lift "Lift end"' and the moment when the monkey receives the reward "Reward."

To separate the different generators that integrate the LFP signal, we used a blind source separation approach using ICA. Before applying ICA, we identified frequency bands of interest for each monkey based on power spectral density (PSD) changes around movement onset (Figures 1B and 1D). Visual inspection of LFP ICs revealed consistent peaks of activity coinciding with known behavioral markers across multiple frequencies (Figure S5). We chose to focus on the 0.1–3 Hz band (Figure 2A) because this frequency presented clear unimodal peaks associated with behavioral events (compared to multimodal peaks observed for higher frequencies, possibly reflecting harmonics). For each recording session (10 in total), ICA produced 192 components (matching the number for recording electrodes). To select specific ICs for analysis, we first identified peaks exceeding a threshold of 3.5 standard deviations. ICs with where the number of peaks was similar to the number of trials were examined further. Typically, this step eliminated over 90% of the total ICs. For reference, Figure S6 presents a scatter plot depicting the number of peaks versus the variance of each IC in each recording session.

Once the subset of ICs to be analyzed was determined, the next step involved ordering them to establish correlations with the observed neural activity during each phase of the task. In ICA, the criterion for selecting the most informative ICs primarily depends on the specific characteristics of the problem being investigated. In our study, we focused on identifying ICs that exhibited consistent patterns of activity across trials and recording sessions. To determine this, we devised a classification metric that incorporated measures of temporal consistency and peak amplitude, with reference to known behavioral markers (for a full description, see method details). By utilizing these metrics, we aimed to objectively assess and rank the relevance of the ICs in capturing the desired neural activity patterns. It is important to note that

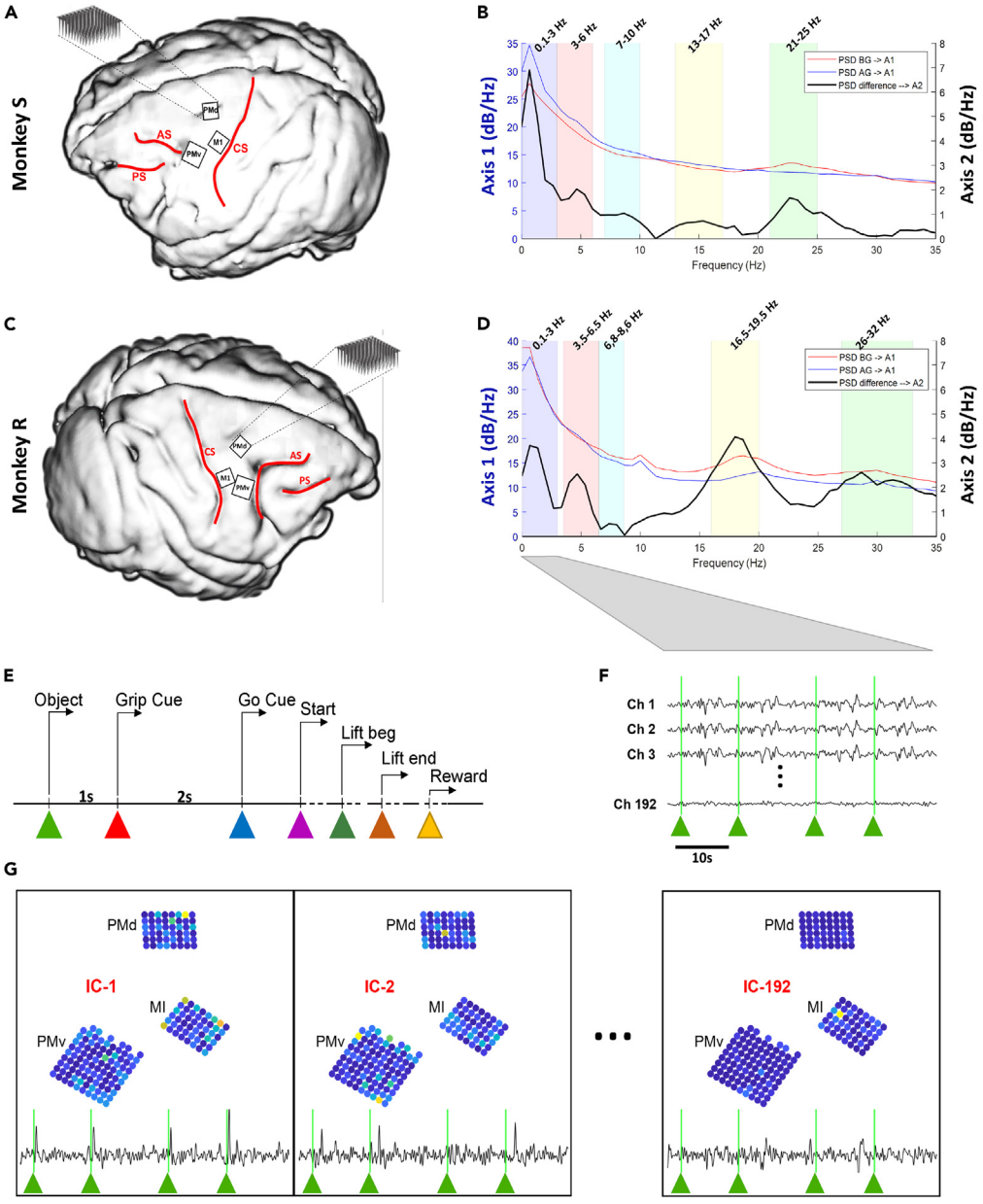

Figure 1. Blind source separation of LFP signals using ICA

(A and C) Placement of the three microelectrode arrays on the left hemisphere of monkey "S" and arrays on the right hemisphere of the monkey "R" respectively. CS, Central sulcus; AS, arcuate sulcus; PS, principal sulcus.

(B) Absolute value of the difference in power spectral density (black line on axis 2) for monkey "S" obtained by subtracting the PSD of the 1.5s segment after the start of the movement (AG blue line on axis 1) and the PSD of the 1.5s segment preceding the start of the movement (BG red line on axis 1), the following frequency bands were selected 0.1–3, 3–6, 7–10, 13–17, and 21–25 Hz.

(D) Changes in the PSD for monkey "R", 0.1-3,3.5-6.5, 6.8–8.6, 16.5–19.5, and 26–32 Hz were selected.

(E–G) (E) Task timeline, showing the seven behavioral markers of the experiment, (F) Low-frequency filtered signal from 0.1 to 3 Hz (192 channels), (G) Signal separation using independent component analysis (ICA) and topographical map of the weights contributing to different independent components.

our analysis was limited to all known events that were recorded during the task, since these could be objectively aligned and verified. It is possible that other 'orphan' peaks are associated with other external variables or internal states that were not measured.

Low frequency ICs associated with each task event displayed highly stereotyped waveforms (Figure 2B) and specific latencies with respect to the externally recorded event markers (Figures 2D and 2E). This pattern was consistently observed across all sessions in both monkeys. IC peaks associated with movement event markers (i.e., start of movement, begin lift, end lift) displayed the shortest and least variable latency for

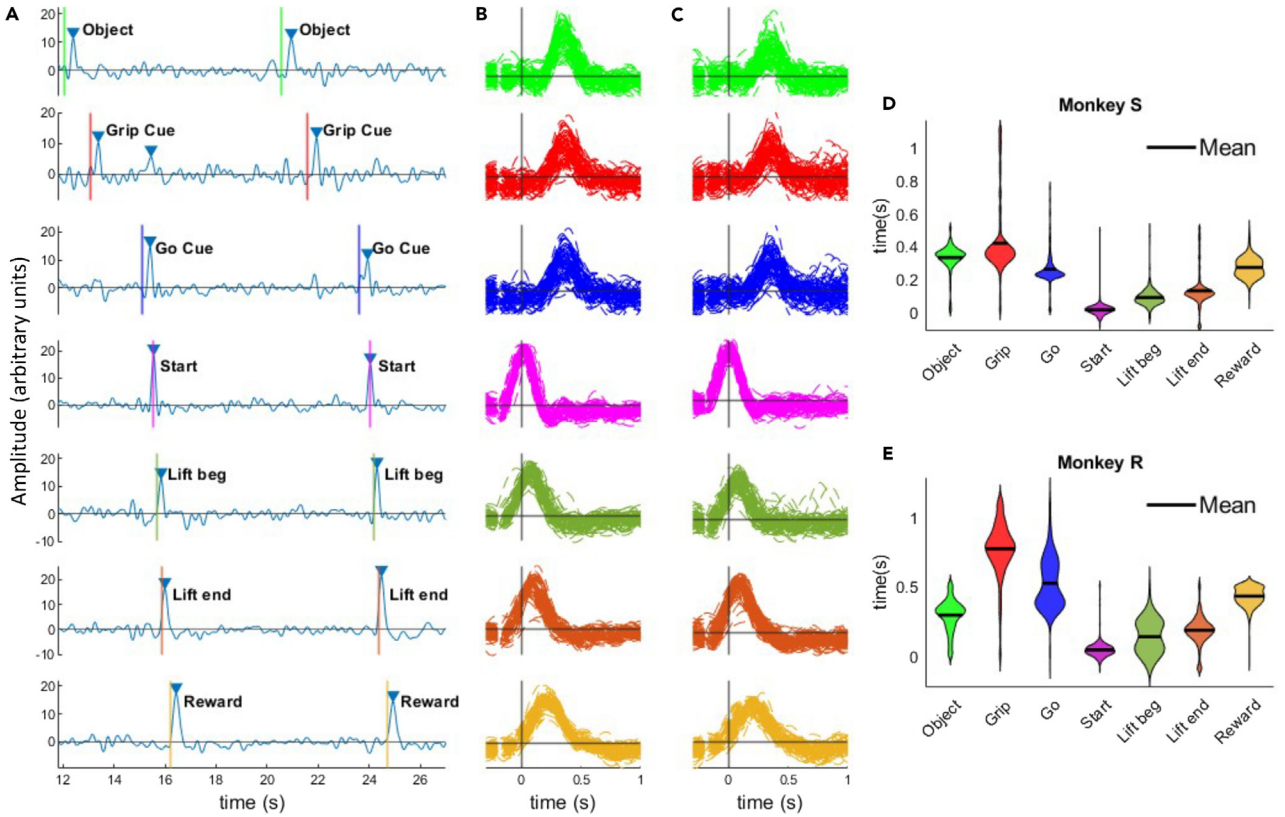

Figure 2. LFP ICs display peaks time-locked to specific task events

(A) Extracted ICs, vertical lines represent external task event markers.

(B) IC waveforms for individual trials in session 1 of monkey "S", each line represents one trial (N = 91) and each color represents ICs aligned with different behavioral events.

(C) IC waveforms for individual trials in session 2 using the W matrix from session 1, each line represents one trial (N = 103).

(D and E) Violin plot of IC peak latency with respect to the external event markers. The data presented in panels (C and D) combine trials from 5 sessions in each monkey. For each dataset, 50% of the data was used to obtain the unmixing matrices and the remaining 50% for testing.

both monkeys, while the planning stages (i.e., object presentation, grip cue, go cue) displayed greater within and between subject variation (Figures 2D and 2E).

Event related ICs tended to be relatively stable across time. This robustness is evident in Figure 2C, where the ICs were extracted from session 2 of monkey "S" using the unmixing matrix (W) obtained from session 1 of the same monkey, producing similar waveforms. This finding highlights the generalization power of the method, indicating that it can effectively capture consistent patterns even when applied to different recording sessions. To further support this point, Figure S7 shows different versions of the ICs derived from datasets comprising 80%, 60%, 40% and 20% of the available data from a given session. In terms of Pearson's correlation coefficient, when 60% of the data is used, there is degradation in the quality of the ICs of 5.8%. This observation underlines the high degree of robustness of the method.

ICs for task stage detection

As already mentioned, the isolated ICs present a prominent peak of activity associated with each task stage external event marker. We hypothesized that these ICs represent neural events (likely related to synaptic influences) that mark influx of information related to external events. For this analysis, the ICA event related to the external event would be the one nearest in time, with the largest amplitude and smallest variance in latency. In order to evaluate the informational content and potential utility of individual ICs we attempted to detect the onset of task stages using an amplitude threshold for each associated IC. Figure 3A serves as an illustrative example of how the algorithm operates. To incorporate cross-validation into our analysis, we divided the data into two equal halves. The first 50% of the data was utilized to apply ICA and extract the unmixing matrix W. Subsequently, the remaining 50% of the data was used to evaluate the stage detection algorithm. The onset of task stages was detected whenever the value of the associated IC exceeded a predetermined threshold. The method employed for threshold optimization relies on the geometric mean of the Receiver Operating Characteristic (ROC) curve. For further details regarding this methodology, please refer to the "method details" section, where a comprehensive description of the threshold optimization process is provided. In Figure 3A, the IC associated with object presentation is shown as an example; note that in some trials, the IC peak is present, but its amplitude

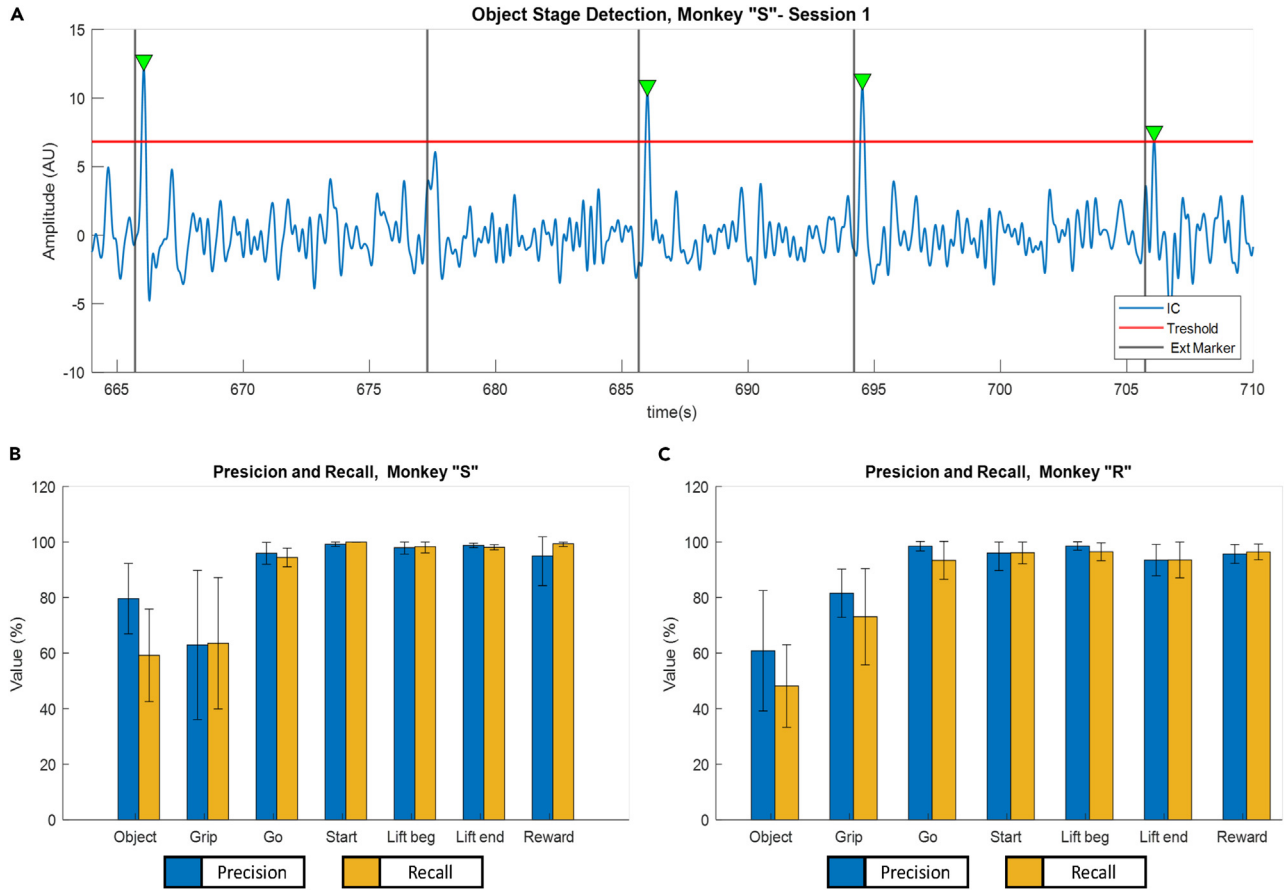

Figure 3. ICs for the detection of task stages

(A) Independent Component corresponding to the object presentation, note that in some trials the characteristic peak of the IC is visible, but its amplitude does not exceed the set detection threshold.

(B) Precision and Recall for monkey "S". Note the greater variability in the detection of the planning stages "Object Presentation" and "Grip Cue", from "Go Cue" to the end of the task, values above 90% are reached.

(C) Stage detection results for monkey "R". Error bars reflect the standard deviation (SD) across the five recording sessions for each monkey. Precision and recall are used in the statistical sense, corresponding to [true positives/(true positives +false positives)] and [true positives/(true positives +false negatives)] respectively.

does not exceed the detection threshold. This phenomenon occurs most frequently in the motion planning stages, which causes the algorithm's efficiency to decrease considerably. For the five stages from "Go Cue" to "Reward," we achieved an average precision of 96.7 $\pm$ 5.2% for "S" and 94.2 $\pm$ 6.0% for "R," while for recall, we achieved 97.5 $\pm$ 2.9% for "S" and 92.8 $\pm$ 6.9% for "R" (Figures 3B and 3C). For the first two planning steps "Object Presentation"' and "Grip Cue" the detection performance decreased to 71.6% and 72.27% for precision and recall in "S" monkey while for "R" monkey we achieved 60.7% and 61.4% for precision and recall. This decrease in performance is due to the amplitude variability in these ICs.

ICs for trial alignment

Aligning neural spiking activity patterns using external event markers (e.g., stimulus or movement onset) is a common practice in neurophysiology, used to measure the time needed to generate an action or for an action to influence neurons in the area being measured. This measurement can be quite variable for a number of reasons, including neural processing time especially for sites that are many synapses away from their source. ICs could potentially be used as intrinsic alignment points, either supplementing or replacing external markers by basing events on internal neural signals that are the signatures of these events near to the neural measurement site. We developed a metric based on the firing rate profile around internal markers and ICs to qualitatively compare external event vs. internal neural marker strategies. The metric used assumes that a better alignment of trials will produce a higher amplitude firing rate profile, i.e., with more defined and prominent peaks and valleys because the actual generator or source is used to align neural spiking activity (for more details, see method details). In Figure 4A the three neurons displaying improved alignment statistics are presented as an example. In one case, the alignment obtained using ICs reveals a new firing pattern: in the third neuron shown in panel Figure 4A, the firing rate using ICs (blue line) shows that the firing pattern presents

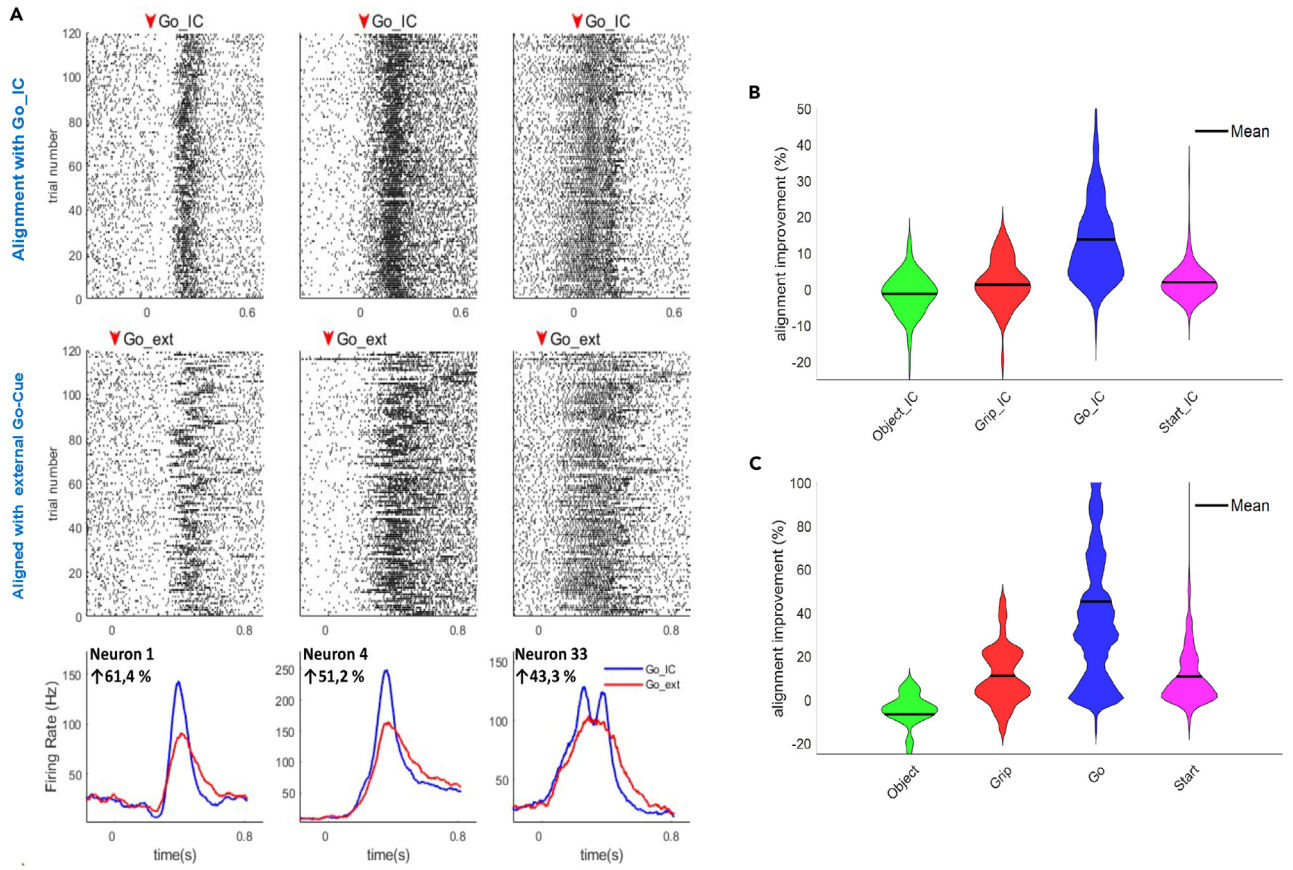

Figure 4. ICs for trial alignment

(A) Spike alignment using external markers vs. ICs, the 3 selected neurons belong to monkey "R" session 1, (N = 119 trials).

(B) Violin diagram of the alignment results for monkey "S", the most notable improvement is obtained in the "Go Cue" stage, in the rest of the stages the results are similar between external markers and ICs.

(C) Violin diagram for monkey "R", in this case ICs yielded improved alignment scores for the "Grip Cue", "Go Cue" and "Start" stages. See also Figures S2–S4.

two peaks approximately 100 ms apart, a pattern that is not observed when aligning the data with an external marker ('Go Cue'). The panels shown in Figures 4B and 4C, demonstrate that the ICs yield alignment metrics on par with or exceed external markers. The average alignment metric improves by 13.8% for the "S" monkey and by 45.2% for the "R" monkey for "Go Cue" events. This alignment improvement suggests that these ICs are a more reliable marker of the internal processes related to the event compared to the external marker. This would help mitigate RT variations that occur in the neural processes that take place between the recording site and the original source of the influence. For the other task stages, the improvement is not significantly different than external event markers, which indicates that the ICs perform as well as the external markers, so they could be used to detect events when external event markers are not available or even detect internal influences that cannot be directly measured externally (see discussion for the possible uses of this result). The results are replicated for monkey "R"; note the improvement not only in the "Go" stage but also in "Grip Cue" and "Start of Movement". For more detailed information, please refer to the supplementary figures. Figure S2 displays three example neurons aligned with respect to the "Object presentation" in monkey S session 1. In Figure S3, we present three example neurons aligned with respect to the "Go Cue" in monkey S session 2. Figure S4 shows three examples of alignment with respect to the "Start of Movement" in monkey S, session 1.

Spatial localization of activity driving ICs

Each LFP component or generator is defined by a spatial and a temporal element. The temporal element consists of the waveforms of each IC that are useful to identify times or events of interest in the course of neuronal activity Figure 2. In contrast, the spatial element consists of the set of electrodes (corresponding to a specific recording site in the cortex) and their assigned weights, which represent the contribution of that electrode to a specific IC (Figures 1G and 5A). The spatial distribution of these weights can be compared to anatomical landmarks and help locate cortical regions associated with specific IC sources. We assessed the relative contribution of M1, PMd, and PMv neural activity to the ICs belonging to each task stage using a Monte Carlo approach (Figure 5A) to test the null hypothesis that IC weights are randomly distributed among the specific sites sampled across cortical surface. In order to calculate the expected distribution of weights under the null hypothesis,

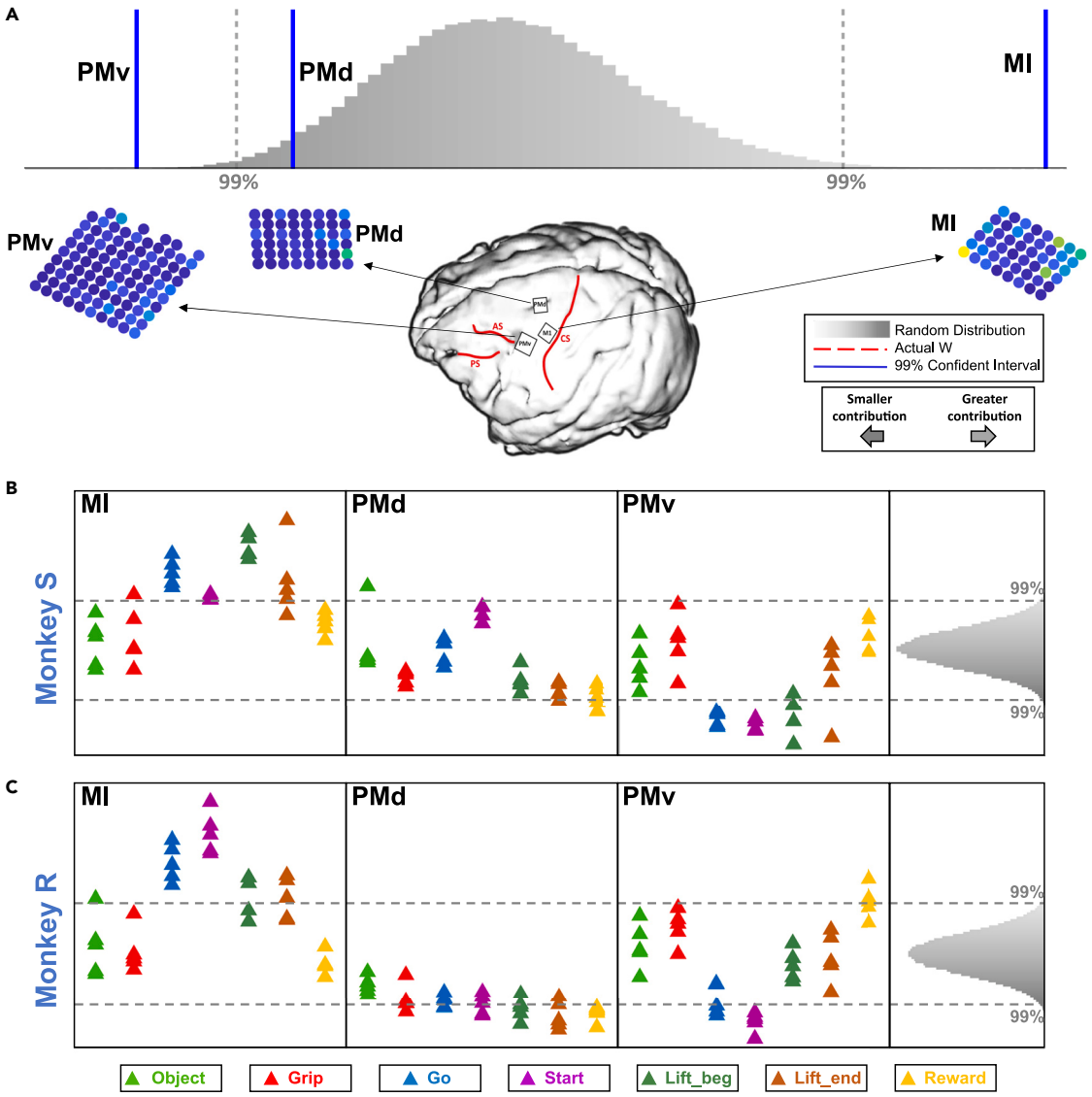

Figure 5. MI, PMv, and PMd differentially contribute to LFP ICs across different task phases

(A) Monte Carlo approach used to evaluate the relative contribution of each cortical area to specific ICs including a topographical map of the weights associated with a specific LFP IC in one sample session, and the expected chance distribution of average IC weights obtained by randomly shuffling 10,000 times. The dotted lines represent 99% confidence intervals, and the continuous blue lines represent the actual average value observed within each region.

(B) Relative contribution of each cortical area to the seven selected ICs in monkey "S". Each colored triangle represents the mean value of the ICA weights, in each phase of the movement and in each recording session relative to the expected chance distribution in light gray. For example, the triangles in cyan represent the "Lift beg" component, it can be observed that for this component the MI contribution is higher than the expected value by chance, in PMv it is lower and in PMd it is within the expected range by chance, this pattern is similar in all five recordings.

(C) Relative contribution of each cortical area to the seven selected ICs in monkey "R". In general, it can be observed that the preparatory activity is distributed in the three areas while in the execution stages the activity is mostly concentrated in the MI.

we performed 10,000 random shuffles and calculated the mean value for each of the microelectrode arrays. To estimate the level of contribution of each region to a specific IC we compare the expected chance distribution with the actual average value within each area. We categorized the neural activity into three levels relative to the chance distribution: "Greater contribution to IC," "Within expected chance," and "Smaller contribution to IC," the threshold separating these three levels corresponds to the empirical ±99% confidence limit (vertical lines in Figure 5A).

A representative example of topographic analysis is shown in Figure 5A. For this specific component, it is possible to identify visually that the largest weights contributing to the IC are mainly concentrated in MI, while in PMd and PMv, the contribution is lower than expected by chance. The data reported in Figure 5A statistically validate this assessment, in this panel the orange curve represents the probability

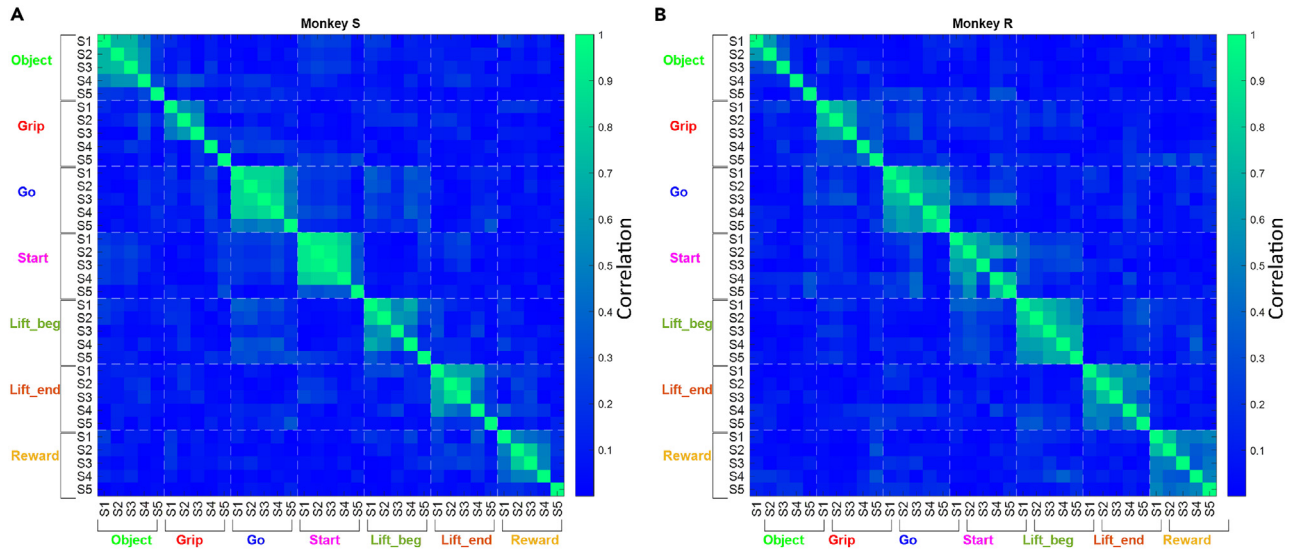

Figure 6. IC weights across the cortical surface display correlated patterns across days

Correlation between topographical activation maps of all stages and all sessions.

(A) Monkey "S", and (B) Monkey "R", in the two plots the components have been grouped according to task stages, S1 to S5 represent each of the recording sessions.

distribution of the randomly shuffled weights and the green vertical line represents the actual mean of the weights within each array. The actual mean of the weights in MI exceeds the 99% confidence limit corroborating the initial visual assessment, while in PMd and PMv the activity remains within and below what would be expected by chance. This procedure was repeated for each component in each recording session.

Overall, the spatial localization analysis shows a consistent pattern over the five recording sessions studied and in both NHPs. In the planning stages, neural activity is distributed over all three areas (light green and red triangles in Figures 5B and 5C). In contrast, the activity is progressively concentrated in MI during the movement stages of the task (blue, magenta, dark green and brown triangles in Figures 5B and 5C). Finally, when the task ends and the monkey receives the reward, the activity is again distributed over the three cortical areas (yellow triangles).

Consistency of activation maps across sessions

This study included five recording sessions for each monkey; for monkey "S," the first four sessions were recorded with a maximum separation of 1 day, and the last recording was recorded after approximately one month. For monkey "R," the first three sessions were recorded with a maximum separation of 2 days, and the last two sessions were recorded after one and two weeks, respectively. The proximity of the recording sessions reduces the likelihood that the array had shifted to slightly different recording sites. This type of motion cannot be measured directly. Comparison of variability over time provides a measure of the stability of the ICA signal. To examine the consistency of the ICs from session to session, we calculated the correlation between maps (i.e., weights assigned to each electrode) of each possible pair of ICs taken from all recording sessions. In consideration of the fact that the polarity of the ICs obtained from ICA is contingent upon the initial values of the unmixing matrix W, we have made a deliberate choice to utilize the absolute value of the correlation for our analysis. By employing the absolute value of the correlation, we concentrate on the magnitude of the correlation without considering the specific polarity of the ICs. Figure 6 shows the results of this analysis: Overall, the correlation between ICs of the same stage present high values while the correlation between ICs coming from different stages present values close to zero. To statistically validate this evaluation, we first separated the values into two groups. Group 1 (G1) includes the correlations between ICs from the same stage but in different recording sessions, yielding 10 values per stage, in total G1 contains 70 values. Group 2 includes the correlation values between ICs from different stages and different recording sessions, yielding 75 values per stage; in total G2 includes 525 values. A Kruskal–Wallis test was then performed and revealed a significant statistical difference between these two groups; Chi square = 123.96, p = 8.65e-29, df = 1 for monkey "S", and Chi square = 142.7, p = 6.64e-33, df = 1 for monkey "R".

In general, correlations for the same ICs tended to be higher for the movement ICs compared to planning stages (Figure 6). For monkey "S" (Figure 6A), the correlation was highest for the first four sessions and lower in the last one, recorded one month later. For monkey "R" (Figure 6B), the correlation in planning stages is strong only between the first three sessions (note that the first three recording sessions were on consecutive days, and the last two were separated by one and two weeks, respectively). The observed pattern in the correlation of the activation maps suggests that for this frequency band (0.1–3 Hz), the neural subnetworks involved in the generation of the ICs present

a high similarity in their topographic structure when the recordings were close together, and this similarity decreases over time. The source of this variation cannot be determined: it could be movement of the electrode, changes in the state of the network, behavior, or other factors.

Decoding object and grip type

So far, we have presented a set of ICs (7 out of 192) which are linked to the stages of the motor task. We then asked whether any of the ICs contained grip- and object-specific information. We used as a discriminant feature the amplitude of the whole set of ICs (192) obtained by ICA to test whether this information was sufficient to classify grip and object type using standard population decoding methods. These results help clarify the nature of the ICs (what information they represent) and are informative with respect to their use in Brain-Machine Interface system development.

For each segment we used a 50 ms sliding window with 50% overlap to continuously estimate the discriminative power of the extracted LFP features. To avoid misalignment due to varying reaction times, the sliding window was aligned either to object presentation (movement planning) or object contact (movement execution). The feature vector was created with the average amplitude of each IC and the decoding was performed using an LDA classifier trained on 70% of the data and tested on the remaining 30% (see method details). Classification results over time for object and grasp type are shown in Figure 7 Before task initiation, for all monkeys, the mean performance for a given classification type was within the chance level range (evaluated using a Monte Carlo approach with 200 random shuffles of the trial labels).

In agreement with previous studies (Bansal et al., 2011[7]), our results show that these low frequency LFPs contain information reflecting the target object and grasp type (Figure 7). Grip and object information was consistently decoded well above chance levels for both animals around the time of contact with the object. Decoding was more variable during the instructed delay, with monkey S presenting more robust decoding than monkey R. This discrepancy could be the result of different behavioral strategies, the neuronal populations sampled by each set of arrays, or attentional effects.

Another particularly interesting aspect to note is the data shown in Figures 7G and 7H panels. Figure 7G shows the histogram of the classification results of the grip type when working with object B only using attributes extracted from a single IC at a time. The remarkable thing about this histogram is the existence of ICs with high information to identify the type of grip used. For this specific case, the IC with the highest discriminant information is IC-141. Figure 7H shows the waveform of IC-141 which demonstrates that the proposed method is also able to extract/isolate ICs with high information content to classify events (objects and/or grips). In other words, ICA in low-frequency LFPs in addition to isolating event-independent ICs (temporal markers), is also able to extract a set of event-dependent ICs (ICs with high discriminative information).

Distributed neuronal activity

The observed ICs were spread over several sites, that is, they present a non-confined spatial pattern. We next evaluated the relative contribution of sets of electrodes to the results. We therefore examined whether there are dominant channels for each IC, i.e., small groups of channels with disproportionately large contributions without which the IC loses its main characteristics. For this purpose, we measured the correlation between the final IC (192 channels) and a series of components created by adding progressively from 1 to 192 channels. To illustrate, Figure 8A shows the "Start" component and four waveforms of the same component created using only the top 15, 30, 45, and 60 channels. The addition of channels was done starting with the ones assigned the highest weight by ICA.

Our results demonstrate that the neuronal activity that makes up the ICs tends to be distributed across multiple channels in the three cortical areas studied rather than being concentrated in a few channels or a small defined cortical region. Figures 8B and 8E shows that correlation with the final IC gradually increases as more channels are added (with ~50 channels required to reach a correlation coefficient of 0.5), showing that there are typically no highly dominant channels but instead many cortical sites contribute to each IC. It can also be observed that the correlation curve for movement stages converges more rapidly, this pattern suggests that during movement fewer channels are required to reach the final IC. This analysis also corroborates the hypothesis that neural activity in the planning period is distributed over M1, PMv, and PMd while it is more concentrated in M1 during movement. In panels, Figures 8C and 8F (planning) the contribution of each area is roughly similar, while in panels Figures 8D and 8G, (execution) the contribution of M1 is higher.

The curves shown in Figures 8D and 8G demonstrate that in the two monkeys in the execution stages the percentage contribution of MI (blue line) to the conformation of the ICs is higher than PMd and PMv, this result corroborates the analysis and results presented in Figure 5. An interesting aspect, which could be the subject of a more detailed analysis, is the fact that the components of the execution stages converge faster in monkey "S", which means that they need fewer channels to reach a higher similarity with the final waveform. Another relevant detail can be seen in Figure 8F, in this panel it can be observed that for the "R" monkey about the 30 most important channels for planning come from PMv in contrast to the "S" monkey where the contribution of the three areas is similar. These differences may suggest that despite the differences in the processing and/or "wiring" of the neural networks, ICA is able to extract the relevant ICs for each stage. This analysis, in addition to giving us an idea of how the regions studied contribute to the conformation of the ICs, allows us to rule out the hypothesis that the ICs may derive from some external artifact affecting a reduced set of channels.

Aggregating the electrodes by blocks, i.e., all the electrodes belonging to the same array, can give us an idea of the contribution of each cortical region. For monkey "S" the correlation for the planning stages reaches MI = 0.27, PMd = 0.31 and PMv = 0.70 while for the movement execution stages MI = 0.53, PMd = 0.39 and PMv = 0.64. On the other hand, for monkey "R" in planning, the mean correlation is MI = 0.06, PMd = 0.35 and PMv = 0.66, while for the task execution stages MI = 0.53, PMd = 0.39 and PMv = 0.62. Again, these results

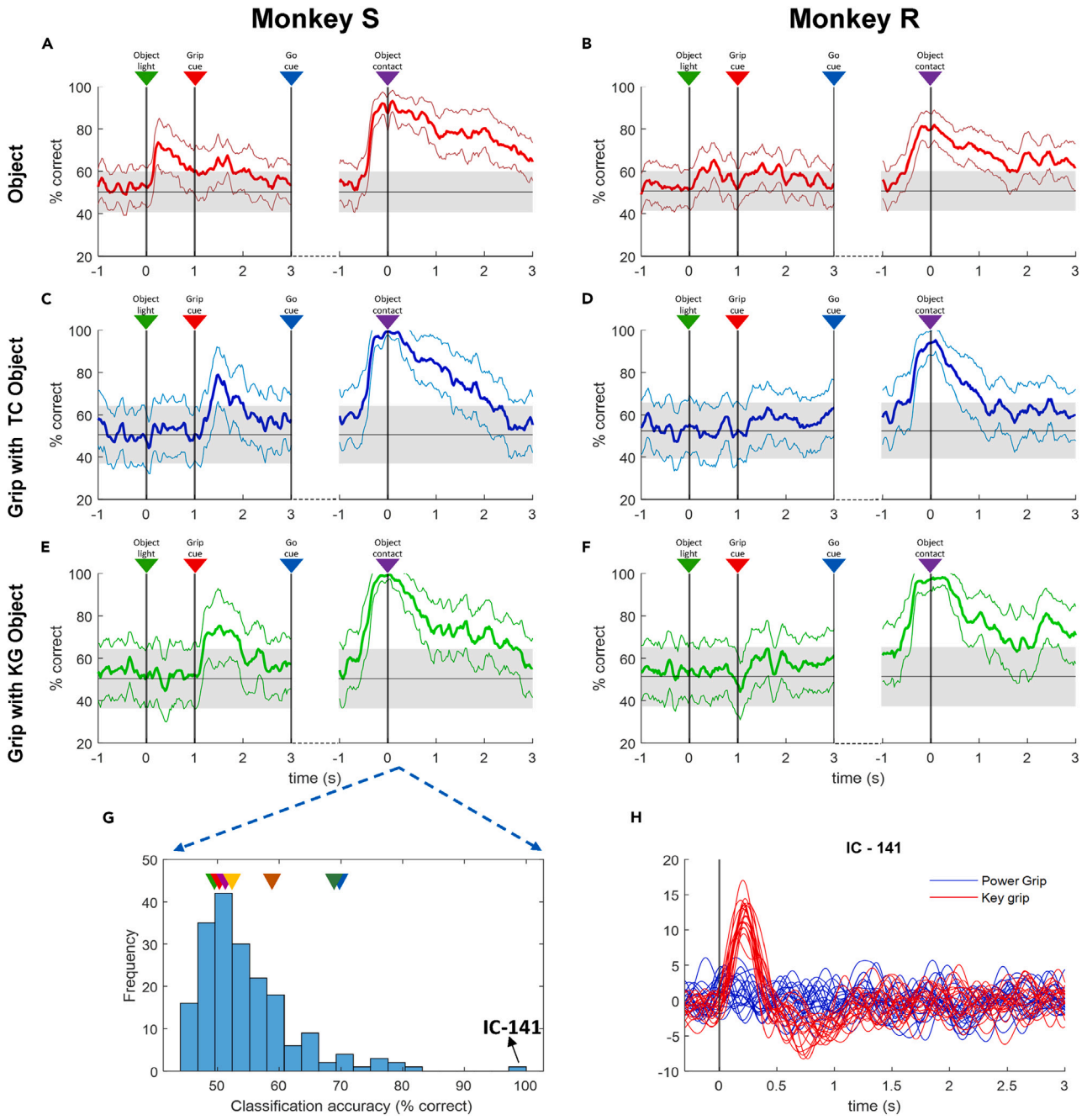

Figure 7. LFP ICs contain information related to target object and grasping strategy

An LDA classifier with 70% training and 30% test data were used to predict object type and grasping strategy. Features were extracted from the low frequency LFP band using a 100 ms sliding window with 50% overlap. The feature vector was created using the average amplitude of each IC. The results for each monkey are shown separately (mean of 5 sessions for each animal). The standard deviation is presented with thin colored lines obtained with 200 runs. The shaded horizontal bar represents the probability of chance +/− one standard deviation.

(A and B) Object Classification.

(C and D) Classification of the grip when the task was performed with the "A" object.

(E and F) Classification of the grip when the task was performed with "B" object.

(G) Histogram of the grip classification results using only one IC at a time when the task was performed with the "B" object. Note the IC-141 which has a very high discriminant power.

(H) Waveform of IC-141, each line represents one trial.

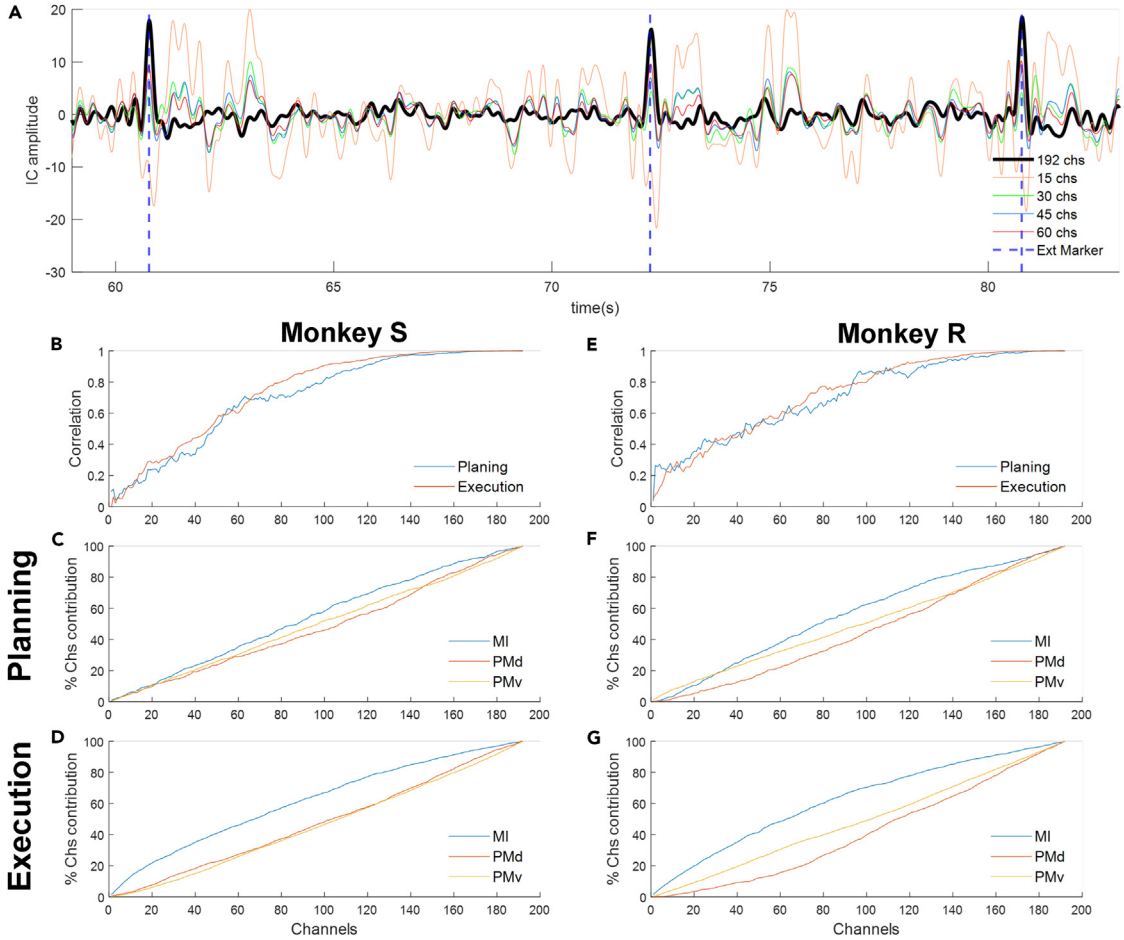

Figure 8. LFP ICs represent signals distributed across multiple recording channels

(A) The "start movement" IC obtained using 192 channels (thick black line) is compared to the combination of the 15, 30, 45, and 60 channels with the highest assigned weights. It is important to note that as channels are added, the characteristic peak of the component is emphasized, while the activity lateral to the peak is flattened.

(B–G) Subplots (B and E) the correlation between the final component and the waveforms created by adding channels. The more similar the waveforms compared, the higher the correlation. It is important to note that the components of the execution stages converge faster, which means that they need fewer channels to achieve greater similarity with the final waveform. Panels (C and F) show the contribution of each area to the conformation of the components in the planning period. Panels (D and G) show contribution of the three cortical regions to ICs associated with movement execution.

suggest that the greatest influence of PMv is observed in the planning stages, while MI appears to be more influential in the execution stages.

DISCUSSION

Large numbers of neurons contribute to the generation of LFPs, even when recorded from a single microelectrode. Sources for low frequency LFPs are a reflection of synaptic current flow, where the inputs could be of local or distant origin. Previous studies have shown that blind source separation techniques allow the identification of generators in multilayer recordings.[31,32] Here, we validate the feasibility of this approach in MEA recordings (192 channels) to measure across several cortical areas, assuming the existence of spatially static independent sources in the lower frequencies of the LFP. We demonstrate that an accurate and robust separation of constitutive signals from LFPs is possible and that it is possible to assign specific ICs (Figure 2) to specific planning and execution stages of voluntary movement. These LFPs show a complex spatial pattern that relates to discrete events for a task that requires planning to grip an object with a specific grasp type and then performing that action. We found that each IC is distributed across multiple electrodes, typically in multiple areas and that the specific information contained in each IC could help identify critical time points in neural processing and aligning trials. We also found that features extracted from the complete set of ICs provide helpful information for object and grasp classification.

We were able to isolate ICs associated with specific behaviorally relevant events that exhibit the following characteristics: (1) In the 0.1–3 Hz band, the ICA isolated seven ICs representing each task stage. (2) Isolated ICs show high temporal consistency within the same session and between sessions recorded on different days. (3) Our analysis revealed that low-frequency ICs can be used for task stage detection and epochal alignment with performance comparable to experimentally controlled external event markers. (4) Localization of neuronal activity assessed by a Monte Carlo approach revealed neuronal activity, instead of originating from small clusters of electrodes confined to specific regions, occurs in a distributed manner at many spatially distributed electrodes. (5) Correlation analysis of the neural activity maps showed that the topographical distribution of electrode weights generating the ICs are highly similar between different sessions. This similarity decreased when comparing sessions separated by many days. (6) Low-frequency ICs contain sufficient information to classify objects and grasp types successfully. In addition, we also demonstrate that the proposed method is able to isolate event-dependent ICs, i.e., ICs whose waveform depends on the type of object or grasp being used.

ICs as internal markers

The unique characteristics of the ICs related to specific task phases lead us to hypothesize that these signals may represent intrinsic markers associated with the arrival of information originating from distinct sources impinging on MI/PM networks. Before explaining the reasons that lead us to this hypothesis, it is essential to highlight the structure of the experiment. The experiment was designed so that neural processing required the integration of two different types of information (1) information directly related to the object geometry and (2) information related to the grasping strategy through a learned stimulus-response association.[30] In addition, the temporal sequence of the task was designed to include periods of delay between instructions (Figure 1E). This approach allows us to independently analyze the neural activity evoked by object presentation, the neural mechanisms related to selecting a specific type of grasp, and the brain activity governing the execution of the movement.

The first characteristic supporting the hypothesis of ICs as indicators of a functional state transition in the network is their stage specificity. This feature is easily identifiable in Figure 2A where it is notable that each IC shows an activity peak exclusively when one of the seven task stages is in progress, e.g., IC-1 shows a prominent peak only after object presentation and is approximately flat afterward. Considering that the "Object presentation," the "Grip Cue," and the "GO cue" are visually presented instructions, the stage specificity observed in the isolated ICs allows us to state that these signals are different in nature from the signals found in previous work such as the P300 or the VEPs, which do not exhibit stage specificity, e.g., the P300 appears when an unusual stimulus is presented regardless of the type of stimulus whether visual, auditory or tactile. VEPs are also not task-stage specific here, the neural response depends on the frequency at which the visual stimulus oscillates. The fact that the ICs are different for each stage and that the activation maps associated with each IC have different topographic distributions suggests that each IC represents a different functional component and origin.

"Condition independence" is another feature of the event related ICs (Figure 2). which may help to understand their role in cortical processing. We use the term "condition independence" to mean that the waveforms (i.e., their amplitude and latency) associated with individual ICs are relatively consistent, and do not seem to change with, for example, the shape of the object presented or the type of grip performed (Figure 2). In other words, the ICs provide valuable information about when a specific stage is in progress (i.e., the type of computation taking place) but contain little information about the object or type of grasp (i.e., the final output of said computation). A reasonable hypothesis is that the ICs represent critical points that reflect sudden changes in the computations taking place within the observed network, driven by the arrival of different types of information, e.g., object geometry, grasping strategy, transition from planning to execution, direction of movement, etc. Our findings are in agreement with previous reports of condition ICs modulated by time in frontal networks.[33] However, considering that ICA operates under the assumption of statistically independent and topographically static or quasi-static sources the specificity of the signals we have identified suggests that they represent statistically independent inputs to the network, rather than a unified, diffuse, time-varying driving signal. One possible interpretation is that the condition IC identified in previous work could be equivalent to the sum of the task stage specific ICs we observe.

Finally, another property of ICs that reaffirms the idea that ICs reflect "Internal Behavioral Markers" is that each IC has a specific latency and variability. Figures 2D and 2E, illustrates the characteristic latency for each stage. For example, in monkey "S" we have Object $\approx$350 ms for Grip Cue $\approx$500 ms and Go Cue $\approx$250 ms. Considering that all instructions are visual, these differences in latency and variability suggest that these ICs do not represent a visual evoked potential but rather that they represent neural changes from different processes with different cognitive loads. Under this hypothesis, we could explain the high latency and variability observed in the "Grip Cue" component. Upon receiving the grip cue, the monkey must perform an arbitrary stimulus response association, combining color of the light with the shape of the target object in order to select a grasping strategy. We hypothesize that the additional cognitive load may require a slightly longer processing time, reflected in the increased latency for the "Grip Cue" IC.

ICs for the development of BCIs

Understanding the neural signals underlying motor control is a critical step in the development of brain-computer interface systems aimed at improving the quality of life of people with motor disorders. Trial alignment is an essential step in signal processing both to study neural function and to develop reliable BCI decoding systems.[34]

Usually, BCI applications require neural data to be aligned with the user's (assumed) intention to move in order to train a decoder for real-time BCI applications. Although the timing of instruction cues can be carefully controlled, there is no direct way to measure movement onset in a person who is paralyzed. Depending on the severity of motor impairment, it may be possible to measure motor event potentials or other

related signals, but setting up the additional sensors required is cumbersome, inputs could be subject to other sources of variability and analysis requires trial averaging, obviating single trial processing. Our results suggest that ICs provide important complementary information to external behavioral markers. Specifically, the data shown in Figure 4 demonstrate that alignment using ICs performs as well as or better than alignment using external markers. With the parameters and analysis strategies used here, the stage that presented the most relevant improvement is the "Go Cue" stage with average increases in signal amplitude of 16.2% for monkey "S" and 32.8% for monkey "R". Another significant aspect of the alignment using ICs is that small changes in the alignment could lead to the discovery of new firing patterns, as in the case of neuron 33 presented in Figure 4 in which it can be noticed that using the ICs as alignment reference the firing pattern changes significantly, providing more accurate information about the neuronal behavior. It is likely that further study of these ICs could lead to the ability to extract additional or more impactful features from these data. In addition to the potential use of ICs as temporal reference points for trial alignment, we believe that the method proposed here could serve as a preprocessing tool for the application of other techniques such as LFADS[6,35] in which an input variable is the recorded neural spike, thus better-aligned trials could lead to better performance of the algorithm.

Another critical aspect in the study of neural signals is the variability of the response of individual units. Usually, neuronal responses such as spike firing rate, LFPs, and even larger scale brain activity such as EEG vary significantly across trials even under identical external experimental conditions.[36,37] In motor tasks guided by visual cues, such as the one we have studied in this work, differences in reaction times, the speed of execution, grip shape, trajectory, and other aspects vary across trials, causing differences in neural activity patterns. There is a wide range of research focused on explaining the causes of variability, ranging from the recording device (i.e., electrode micromovement, cell loss or tissue reaction), to the dynamics of the brain itself, such as the stochastic character of synaptic transmission,[38] the dynamic shifts linked to neuronal adaptation,[39] and neuroplasticity.[37,40] Regardless of the causes of variability, this problem must be rigorously addressed to achieve reproducible results and stable systems.[41] The ICs described here could be a valuable tool to generate more stable signals in the medium and long term; mitigating either the loss of the recording of a few neurons or micromovements of the sensor over time.

For real time BCI operation, reliable detection of shifts in task stages is very important for stable, reliable performance. The results presented in Figure 3 demonstrate that isolated ICs are highly effective in detecting at least some task stages with high temporal precision. It was shown that for the stages corresponding to the task execution, the percentage of precision and recall exceeded 95% (reaching 100% in some cases). For the planning stages, the performance decreased to approximately 60%. This decrease in performance is due to the variability of the amplitude of these two ICs. This drawback might be overcome by including an adaptive threshold based on a moving window system or using other analytical approaches. Although it is still necessary to test the process in other types of tasks and include more subjects, these initial results are promising and suggest the potential usefulness of lf-LFP in experiments in which environmental instrumentation is not feasible or even, as part of BCI systems outside experimental settings. ICs in the planning phases of the task could also help identify covert neural states, especially in severely paralyzed people for whom it is difficult to assess intended actions. For example, in the object presentation phase, we can precisely record the moment when the object lights up, but we do not know if the monkey paid attention to the signal. However, ICs could provide information that could help to identify this event: Our results suggest that a peak detected for the corresponding IC after object presentation would indicate the arrival of visual information in motor cortex. A similar analysis can be developed for the ICs corresponding to the Grip Cue and Go Cue stages.

Another aspect to highlight is spatial consistency. Figure 6 demonstrates that the neural networks involved in the generation of the lf-LFP ICs remain stable across trials and recording sessions. Our dataset includes sessions on consecutive days and separated by several weeks. Figure 6 shows that the spatial correlation of the generator networks decreased over days. On consecutive days, the correlations are sufficient to use the unmixing matrix "W" on one day to isolate components from another. This feature may also be helpful for brain-computer interfaces, since the rate of reorganization of the generator networks appear to be low (around days or even weeks), which would reduce the need for system recalibration[42,43]

Finally, it should be noted that working with LFPs is relatively straightforward and computationally efficient relative to spike train analysis. For example, a sampling frequency of 250 Hz is sufficient for LFP analysis, as opposed to the original frequency of 30,000 Hz required for single unit analysis. Furthermore, it is important to note that signal preprocessing involves only bandpass filtering, without the need for spike sorting, channel selection, or trial selection, and that ICA is an unsupervised process, i.e., we make no assumptions about the task and do not need to label trials beforehand. Additionally, it is worth mentioning that this type of source separation is perfectly feasible for real-time signal analysis, as the computationally expensive process only takes place in the "training" stage. Once the unmixing matrix "W" is obtained, the only step necessary for the separation of the LFP components is the multiplication of W by the recorded data, which has a low energy cost and a low computational demand capable of being performed in real time.

Future work

Functional specialization and anatomical segregation suggest that the brain is organized as a distributed, hierarchical network of networks. The functioning of such a modular system implies the existence of a highly complex short- and long-distance communication system, which must be able to selectively enable/disable communication pathways to efficiently direct signals to its target neurons while preventing irrelevant signals from being transferred and interfering with the processing task.[44] In cell-to-cell communication (short distance), the most influential factors are the synaptic processes regulated by numerous electrochemical mechanisms that ensure that the message is timely and accurate. By contrast, a large body of research suggests that long-distance communication is based on the parameters of neuronal electrical oscillations.[45–48]

A neuron has a stable geometry however it can function as many different current sources depending on the subset of synapses activated at each instant.[12,49] Therefore, due to the number of neurons and their microscopic nature, which can be combined in innumerable spatial configurations, precisely determining the elementary units and conduction pathways associated with an oscillator or, in our case, with a specific IC is a very complex process that probably requires cytoarchitectonic modeling of the structures involved in the process. However, we can highlight some hypotheses and theories that give us a global idea about the origin of isolated ICs.

The most obvious characteristic that we could argue is that the units that constitute the generating networks of the ICs must present temporal synchronization so that their potentials are in phase, and when combined, they do not cancel each other but rather produce potentials large enough to be measured. However, previous studies have proposed that synchronized neuronal group activity is not sufficient to produce measurable field potentials. It has been shown that some of the most decisive factors in the amplitude, polarity and extent of LFPs lie in the spatial domain. Most influential are the geometry of individual neurons, their three-dimensional arrangement, and the distribution of activating synaptic inputs in individual cells and in the population as a whole. Combinations of these factors make LFPs large or small, positive, or negative, reaching locations far from the source or remaining local.[11,50,51]

At first glance, it would be logical to assume that the functional neuronal groups that generate our ICs are confined to defined spatial regions; however, our data demonstrate that this is not necessarily true. The activation maps in Figure 5 and the data shown in Figure 8 suggest that the neuronal activity associated with each IC is distributed across multiple electrodes, sometimes spanning all cortical areas examined. Therefore, for ICA to successfully isolate ICs, it is necessary for the sources to remain spatially static and for propagation delays between their constituent elements to be minimal. Based on this background, one hypothesis to explain our results is that the motor cortex comprises small anatomically/functionally distributed groups whose information transfer mechanism necessarily occurs through axonal fields.

One possible interpretation is that the ICs we observed are the result of temporally coordinated inputs to the densely interconnected motor/premotor frontal network originating from relatively distant sources. For example, information reflecting object geometry originating from the parietal lobe could account for the IC associated with object presentation. The set of relevant parieto-frontal projections could represent a statistically independent drive to a subset of neurons across the three cortical areas examined. In this sense, the activity peak in this IC could be interpreted as the engagement of a multi-area subnetwork processing object related information. Other cortical (or subcortical) projections could account for the remaining ICs: for example, the prefrontal cortex could be associated with responses to arbitrary stimulus response associations (in this case, the grip cue). Future studies could further test this hypothesis by examining the effects of selective inactivation of different areas on ICs identified in frontal networks. Whether similar mechanisms are evident in a broader range of sensory and association areas also remains to be explored.

Our analysis shows that LFP-ICs can be used to improve the alignment of spike trains relative to the standard practice of using externally labeled events. This suggests that it may be possible to extract similar ICs directly from spiking data. This analysis will entail a different set of challenges and considerations, as the granularity of neuronal firing frequencies requires a larger set of hyperparameters for analysis (e.g., bin width, smoothing kernels, etc.). A detailed comparison of spiking ICs and LFP ICs should therefore be a focus for future research.

Limitations of the study

- The work performed includes the analysis of the components of the LFPs recorded in the motor and premotor cortical regions during the performance of grasping and lifting tasks. We hypothesize that the developed method can be useful in other types of tasks, for example visual or cognitive. However, it is essential to extend the study using other types of signals in order to verify its validity in other fields of neuroscience.
- Our analysis was limited to all known events that were recorded during the task, since these could be objectively aligned and verified. It is possible that other 'orphan' peaks are associated with other external variables or internal states that were not measured.
- The results presented here focus on the 0.1–3 Hz frequency band. However, other bands (e.g., 3-6 Hz) also presented event-related oscillations (Figure S5). These waveforms reveal a temporal synchronization or blocking phenomenon. At first glance, one might consider the 0.1–3 Hz ICs to represent the envelope of the 3–6 Hz band. However, the temporal duration of the 0–3 Hz peak does not align with the duration of the envelope of the 3–6 Hz oscillations, which exhibits a notably longer duration. In addition to the observed synchronization, we also observed an increase in amplitude that coincides with the peak of the 0.1–3 Hz ICs. However, this amplitude increase is only observable during the "Object Presentation" and "Start Movement" phases and is not present in the "Grip Cue" and "Go Cue" phases. Consequently, these disparities initially suggest that the observed phenomenon within the 3–6 Hz range may signify a distinct neural process that requires further investigation.

STAR★METHODS

Detailed methods are provided in the online version of this paper and include the following:

- KEY RESOURCES TABLE
- RESOURCE AVAILABILITY
  - Lead contact
  - Materials availability
  - Data and code availability

SUPPLEMENTAL INFORMATION

Supplemental information can be found online at https://doi.org/10.1016/j.isci.2023.108310.

ACKNOWLEDGMENTS

This work was funded by NIH New Innovator Award: 1DP2NS111817-01. We thank Michelle Nevor, John Murphy, and Allan Rydberg for their assistance with animal training and instrumentation design as well as the Brown University Center for Animal Resources and Education for veterinary support. DOV is supported by the research department of the National University of Loja-Ecuador (27-DI-FSH-2019) and the National Secretariat of Science and Technology of Ecuador (SENESCYT).

AUTHOR CONTRIBUTIONS

Conceptualization, C.V.I., J.P.D., and D.O.V.; Data curation, C.V.I. and J.P.D.; Formal analysis, D.O.V. and C.V.I.; Funding acquisition, C.V.I. and J.P.D.; Investigation, C.V.I. and J.P.D.; Methodology, C.V.I., J.P.D., and D.O.V.; Project administration, C.V.I.; Resources C.V.I. and J.P.D.; Software, D.O.V. and C.V.I.; Supervision, C.V.I. and J.P.D.; Validation, C.V.I., J.P.D., and D.O.V.; Visualization, D.O.V. and C.V.I.; Writing – original draft, D.O.V.; Writing – review and editing, D.O.V., C.V.I., and J.P.D.

DECLARATION OF INTERESTS

J.P.D. is a shareholder in Beacon Biosignals, a neurodiagnostic company and a member of the Board of Directors of PathMaker Neurosciences, Inc.

INCLUSION AND DIVERSITY

We support inclusive, diverse, and equitable conduct of research.

Received: October 9, 2022
Revised: December 8, 2022
Accepted: October 10, 2023
Published: October 28, 2023

REFERENCES

1. Buzsáki, G., and Draguhn, A. (2004). Neuronal Oscillations in Cortical Networks. Science *304*, 1926–1929. https://doi.org/10.1126/science.1099745.
2. Serruya, M.D., Hatsopoulos, N.G., Paninski, L., Fellows, M.R., and Donoghue, J.P. (2002). Instant neural control of a movement signal. Nature *416*, 141–142. https://doi.org/10.1038/416141a.
3. Taylor, D.M., Tillery, S.I.H., and Schwartz, A.B. (2002). Direct cortical control of 3D neuroprosthetic devices. Science *296*, 1829–1832. https://doi.org/10.1126/SCIENCE.1070291.
4. Hochberg, L.R., Serruya, M.D., Friehs, G.M., Mukand, J.A., Saleh, M., Caplan, A.H., Branner, A., Chen, D., Penn, R.D., and Donoghue, J.P. (2006). Neuronal ensemble control of prosthetic devices by a human with tetraplegia. Nature *442*, 164–171. https://doi.org/10.1038/nature04970.
5. Takahashi, K., Kim, S., Coleman, T.P., Brown, K.A., Suminski, A.J., Best, M.D., and Hatsopoulos, N.G. (2015). Large-scale spatiotemporal spike patterning consistent with wave propagation in motor cortex2015. Nat. Commun. *6*, 7169–7211. https://doi.org/10.1038/ncomms8169.
6. Pandarinath, C., Ames, K.C., Russo, A.A., Farshchian, A., Miller, L.E., Dyer, E.L., and Kao, J.C. (2018). Latent Factors and Dynamics in Motor Cortex and Their Application to Brain–Machine Interfaces. J. Neurosci. *38*, 9390–9401. https://doi.org/10.1523/JNEUROSCI.1669-18.2018.
7. Bansal, A.K., Vargas-Irwin, C.E., Truccolo, W., and Donoghue, J.P. (2011). Relationships among low-frequency local field potentials, spiking activity, and three-dimensional reach and grasp kinematics in primary motor and ventral premotor cortices. J. Neurophysiol. *105*, 1603–1619. https://doi.org/10.1152/JN.00532.2010.
8. Heldman, D.A., and Moran, D.W. (2020). Local field potentials for BCI control. Handb. Clin. Neurol. *168*, 279–288. https://doi.org/10.1016/B978-0-444-63934-9.00020-2.
9. Scherberger, H., Jarvis, M.R., and Andersen, R.A. (2005). Cortical local field potential encodes movement intentions in the posterior parietal cortex. Neuron *46*, 347–354. https://doi.org/10.1016/J.NEURON.2005.03.004.
10. Flint, R.D., Wright, Z.A., Scheid, M.R., and Slutzky, M.W. (2013). Long term, stable brain machine interface performance using local field potentials and multiunit spikes. J. Neural. Eng. *10*, 056005. https://doi.org/10.1088/1741-2560/10/5/056005.

11. Herreras, O. (2016). Local field potentials: Myths and misunderstandings. Front. Neural Circ. *10*, 101. https://doi.org/10.3389/FNCIR.2016.00101/FULL.
12. Nunez, P.L., and Srinivasan, R. (2009). Electric Fields of the Brain: The Neurophysics of EEG (Oxford University Press). https://doi.org/10.1093/acprof:oso/9780195050387.001.0001.
13. Makarov, V.A., Makarova, J., and Herreras, O. (2010). Disentanglement of local field potential sources by independent component analysis. J. Comput. Neurosci. *29*, 445–457. https://doi.org/10.1007/S10827-009-0206-Y.
14. Makarova, J., Ortuño, T., Korovaichuk, A., Cudeiro, J., Makarov, V.A., Rivadulla, C., and Herreras, O. (2014). Can pathway-specific LFPs be obtained in cytoarchitectonically complex structures? Front. Syst. Neurosci. *8*, 66. https://doi.org/10.3389/FNSYS.2014.00066/XML/NLM.
15. Senzai, Y., Fernandez-Ruiz, A., and Buzsáki, G. (2019). Layer-Specific Physiological Features and Interlaminar Interactions in the Primary Visual Cortex of the Mouse. Neuron *101*, 500–513.e5. https://doi.org/10.1016/J.NEURON.2018.12.009.
16. Pesaran, B., Nelson, M.J., and Andersen, R.A. (2006). Dorsal premotor neurons encode the relative position of the hand, eye, and goal during reach planning. Neuron *51*, 125–134. https://doi.org/10.1016/J.NEURON.2006.05.025.
17. Lee, J.H., and Van Donkelaar, P. (2006). The human dorsal premotor cortex generates on-line error corrections during sensorimotor adaptation. J. Neurosci. *26*, 3330–3334. https://doi.org/10.1523/JNEUROSCI.3898-05.2006.
18. Dekleva, B.M., Kording, K.P., and Miller, L.E. (2018). Single reach plans in dorsal premotor cortex during a two-target task. Nat. Commun. *9*, 3556–3612. https://doi.org/10.1038/s41467-018-05959-y.
19. Hoshi, E., and Tanji, J. (2007). Distinctions between dorsal and ventral premotor areas: anatomical connectivity and functional properties. Curr. Opin. Neurobiol. *17*, 234–242. https://doi.org/10.1016/J.CONB.2007.02.003.
20. Ninomiya, T., Inoue, K.I., Hoshi, E., and Takada, M. (2019). Layer specificity of inputs from supplementary motor area and dorsal premotor cortex to primary motor cortex in macaque monkeys. Sci. Rep. *9*, 18230–18311. https://doi.org/10.1038/s41598-019-54220-z.
21. Geyer, S., Matelli, M., Luppino, G., and Zilles, K. (2000). Functional neuroanatomy of the primate isocortical motor system. Anat. Embryol. *202*, 443–474. https://doi.org/10.1007/S004290000127.
22. Vargas-Irwin, C.E., Shakhnarovich, G., Yadollahpour, P., Mislow, J.M.K., Black, M.J., and Donoghue, J.P. (2010). Decoding Complete Reach and Grasp Actions from Local Primary Motor Cortex Populations. J. Neurosci. *30*, 9659–9669. https://doi.org/10.1523/JNEUROSCI.5443-09.2010.
23. Cisek, P., and Kalaska, J.F. (2010). Neural mechanisms for interacting with a world full of action choices. Annu. Rev. Neurosci. *33*, 269–298. https://doi.org/10.1146/ANNUREV.NEURO.051508.135409.
24. Afshar, A., Santhanam, G., Yu, B.M., Ryu, S.I., Sahani, M., and Shenoy, K.V. (2011). Single-trial neural correlates of arm movement preparation. Neuron *71*, 555–564. https://doi.org/10.1016/J.NEURON.2011.05.047.
25. Bollimunta, A., Santacruz, S.R., Eaton, R.W., Xu, P.S., Morrison, J.H., Moxon, K.A., Carmena, J.M., and Nassi, J.J. (2021). Head-mounted microendoscopic calcium imaging in dorsal premotor cortex of behaving rhesus macaque. Cell Rep. *35*, 109239. https://doi.org/10.1016/J.CELREP.2021.109239.
26. Kraskov, A., Prabhu, G., Quallo, M.M., Lemon, R.N., and Brochier, T. (2011). Ventral Premotor–Motor Cortex Interactions in the Macaque Monkey during Grasp: Response of Single Neurons to Intracortical Microstimulation. J. Neurosci. *31*, 8812–8821. https://doi.org/10.1523/JNEUROSCI.0525-11.2011.
27. Nelissen, K., and Vanduffel, W. (2011). Grasping-Related Functional Magnetic Resonance Imaging Brain Responses in the Macaque Monkey. J. Neurosci. *31*, 8220–8229. https://doi.org/10.1523/JNEUROSCI.0623-11.2011.
28. Kurata, K. (2018). Hierarchical Organization Within the Ventral Premotor Cortex of the Macaque Monkey. Neuroscience *382*, 127–143. https://doi.org/10.1016/J.NEUROSCIENCE.2018.04.033.
29. Begliomini, C., De Sanctis, T., Marangon, M., Tarantino, V., Sartori, L., Miotto, D., Motta, R., Stramare, R., and Castiello, U. (2014). An investigation of the neural circuits underlying reaching and reach-to-grasp movements: from planning to execution. Front. Hum. Neurosci. *8*, 676. https://doi.org/10.3389/FNHUM.2014.00676.
30. Vargas-Irwin, C.E., Franquemont, L., Black, M.J., and Donoghue, J.P. (2015). Linking objects to actions: Encoding of target object and grasping strategy in primate ventral premotor cortex. J. Neurosci. *35*, 10888–10897. https://doi.org/10.1523/JNEUROSCI.1574-15.2015.
31. Benito, N., Fernández-Ruiz, A., Makarov, V.A., Makarova, J., Korovaichuk, A., and Herreras, O. (2014). Spatial modules of coherent activity in pathway-specific LFPs in the hippocampus reflect topology and different modes of presynaptic synchronization. Cerebr. Cortex *24*, 1738–1752. https://doi.org/10.1093/CERCOR/BHT022.
32. Korovaichuk, A., Makarova, J., Makarov, V.A., Benito, N., and Herreras, O. (2010). Minor contribution of principal excitatory pathways to hippocampal LFPs in the anesthetized rat: A combined independent component and current source density study. J. Neurophysiol. *104*, 484–497. https://doi.org/10.1152/JN.00297.2010/SUPPL_FILE/SUPPMAT.PDF.
33. Kaufman, M.T., Seely, J.S., Sussillo, D., Ryu, S.I., Shenoy, K.V., and Churchland, M.M. (2016). The Largest Response Component in the Motor Cortex Reflects Movement Timing but Not Movement Type. eNeuro *3*, ENEURO.0085–16.2016. https://doi.org/10.1523/ENEURO.0085-16.2016.
34. Dhawale, A.K., Smith, M.A., and Ölveczky, B.P. (2017). The Role of Variability in Motor Learning. Annu. Rev. Neurosci. *40*, 479–498. https://doi.org/10.1146/ANNUREV-NEURO-072116-031548.
35. Sussillo, D., Jozefowicz, R., Abbott, L.F., and Pandarinath, C. (2016). LFADS - Latent Factor Analysis via Dynamical Systems.
36. Masquelier, T. (2013). Neural variability, or lack thereof. Front. Comput. Neurosci. *7*, 7. https://doi.org/10.3389/FNCOM.2013.00007.
37. Chervyakov, A.V., Sinitsyn, D.O., Piradov, M.A., Lebedev, M., Merchant, H., and Sakurai, Y. (2016). Variability of neuronal responses: Types and functional significance in neuroplasticity and neural darwinism. Front. Hum. Neurosci. *10*, 603. https://doi.org/10.3389/FNHUM.2016.00603/XML/NLM.
38. Ribrault, C., Sekimoto, K., and Triller, A. (2011). From the stochasticity of molecular processes to the variability of synaptic transmission. Nat. Rev. Neurosci. *12*, 375–387. https://doi.org/10.1038/nrn3025.
39. Clifford, C.W.G., Webster, M.A., Stanley, G.B., Stocker, A.A., Kohn, A., Sharpee, T.O., and Schwartz, O. (2007). Visual adaptation: Neural, psychological and computational aspects. Vis. Res. *47*, 3125–3131. https://doi.org/10.1016/J.VISRES.2007.08.023.
40. Feldman, D.E. (2009). Synaptic mechanisms for plasticity in neocortex. Annu. Rev. Neurosci. *32*, 33–55. https://doi.org/10.1146/ANNUREV.NEURO.051508.135516.
41. Williams, A.H., Poole, B., Maheswaranathan, N., Dhawale, A.K., Fisher, T., Wilson, C.D., Brann, D.H., Trautmann, E.M., Ryu, S., Shusterman, R., et al. (2020). Discovering Precise Temporal Patterns in Large-Scale Neural Recordings through Robust and Interpretable Time Warping. Neuron *105*, 246–259.e8. https://doi.org/10.1016/J.NEURON.2019.10.020.
42. Rouanne, V., Costecalde, T., Benabid, A.L., and Aksenova, T. (2022). Unsupervised adaptation of an ECoG based brain–computer interface using neural correlates of task performance. Sci. Rep. *12*, 21316–21411. https://doi.org/10.1038/s41598-022-25049-w.
43. Mladenović, J., Mattout, J., and Lotte, F. (2018). A generic framework for adaptive EEG-based BCI training and operation. In Brain-Computer Interfaces Handbook: Technological and Theoretical Advances, pp. 595–612. https://doi.org/10.1201/9781351231954-31.
44. Hahn, G., Ponce-Alvarez, A., Deco, G., Aertsen, A., and Kumar, A. (2018). Portraits of communication in neuronal networks. Nat. Rev. Neurosci. *20*, 117–127. https://doi.org/10.1038/s41583-018-0094-0.
45. Bonnefond, M., Kastner, S., and Jensen, O. (2017). Communication between Brain Areas Based on Nested Oscillations. eNeuro *4*, ENEURO.0153,16.2017. https://doi.org/10.1523/ENEURO.0153-16.2017.
46. Hyafil, A., Giraud, A.L., Fontolan, L., and Gutkin, B. (2015). Neural Cross-Frequency Coupling: Connecting Architectures, Mechanisms, and Functions. Trends Neurosci. *38*, 725–740. https://doi.org/10.1016/J.TINS.2015.09.001.
47. Haegens, S., Nácher, V., Luna, R., Romo, R., and Jensen, O. (2011). α-Oscillations in the monkey sensorimotor network influence discrimination performance by rhythmical inhibition of neuronal spiking. Proc. Natl. Acad. Sci. USA *108*, 19377–19382. https://doi.org/10.1073/PNAS.1117190108/SUPPL_FILE/PNAS.201117190SI.PDF.
48. Klimesch, W., Sauseng, P., and Hanslmayr, S. (2007). EEG alpha oscillations: the inhibition-timing hypothesis. Brain Res. Rev. *53*, 63–88. https://doi.org/10.1016/J.BRAINRESREV.2006.06.003.
49. Kajikawa, Y., and Schroeder, C.E. (2011). How local is the local field potential? Neuron *72*, 847–858. https://doi.org/10.1016/J.NEURON.2011.09.029.
50. Makarova, J., Ibarz, J.M., Makarov, V.A., Benito, N., and Herreras, O. (2011). Parallel readout of pathway-specific inputs to laminated brain structures. Front. Syst.

Neurosci. *5*, 77. https://doi.org/10.3389/FNSYS.2011.00077/XML/NLM.

51. Fernández-Ruiz, A., and Herreras, O. (2013). Identifying the synaptic origin of ongoing neuronal oscillations through spatial discrimination of electric fields. Front. Comput. Neurosci. *0*, 5. https://doi.org/10.3389/FNCOM.2013.00005/XML/NLM.
52. Scheffer-Teixeira, R., Belchior, H., Leão, R.N., Ribeiro, S., and Tort, A.B.L. (2013). On high-frequency field oscillations (>100 Hz) and the spectral leakage of spiking activity. J. Neurosci. *33*, 1535–1539. https://doi.org/10.1523/JNEUROSCI.4217-12.2013.
53. Gips, B., van der Eerden, J.P.J.M., and Jensen, O. (2016). A biologically plausible mechanism for neuronal coding organized by the phase of alpha oscillations. Eur. J. Neurosci. *44*, 2147–2161. https://doi.org/10.1111/EJN.13318.
54. Dimigen, O. (2020). Optimizing the ICA-based removal of ocular EEG artifacts from free viewing experiments. Neuroimage *207*, 116117. https://doi.org/10.1016/J.NEUROIMAGE.2019.116117.
55. Vidal, M., Rosso, M., and Aguilera, A.M. (2021). Bi-Smoothed Functional Independent Component Analysis for EEG Artifact Removal. Mathematics *9*, 1243. https://doi.org/10.3390/MATH9111243.
56. Whitmore, N.W., and Lin, S.C. (2016). Unmasking local activity within local field potentials (LFPs) by removing distal electrical signals using independent component analysis. Neuroimage *132*, 79–92. https://doi.org/10.1016/J.NEUROIMAGE.2016.02.032.
57. Głąbska, H., Potworowski, J., Łęski, S., and Wójcik, D.K. (2014). Independent Components of Neural Activity Carry Information on Individual Populations. PLoS One *9*, e105071. https://doi.org/10.1371/JOURNAL.PONE.0105071.
58. Castellanos, N.P., and Makarov, V.A. (2006). Recovering EEG brain signals: artifact suppression with wavelet enhanced independent component analysis. J. Neurosci. Methods *158*, 300–312. https://doi.org/10.1016/J.JNEUMETH.2006.05.033.
59. Bell, A.J., and Sejnowski, T.J. (1995). An information-maximization approach to blind separation and blind deconvolution. Neural Comput. *7*, 1129–1159. https://doi.org/10.1162/NECO.1995.7.6.1129.
60. Amari, S., Cichocki, A., and Yang, H.H. (1996). A new learning algorithm for blind signal separation. Adv. Neural Inf. Process. Syst. *8*, 757–763.
61. Lee, T.W., Girolami, M., and Sejnowski, T.J. (1999). Independent component analysis using an extended infomax algorithm for mixed subgaussian and supergaussian sources. Neural Comput. *11*, 417–441. https://doi.org/10.1162/089976699300016719.
62. Cheung, Y.M., and Xu, L. (2001). Independent component ordering in ICA time series analysis. Neurocomputing *41*, 145–152. https://doi.org/10.1016/S0925-2312(00)00358-1.
63. Ball, K., Bigdely-Shamlo, N., Mullen, T., and Robbins, K. (2016). PWC-ICA: A Method for Stationary Ordered Blind Source Separation with Application to EEG. Comput. Intell. Neurosci. *2016*, 9754813. https://doi.org/10.1155/2016/9754813.
64. Chaure, F.J., Rey, H.G., and Quian Quiroga, R. (2018). A novel and fully automatic spike-sorting implementation with variable number of features. J. Neurophysiol. *120*, 1859–1871. https://doi.org/10.1152/JN.00339.2018/ASSET/IMAGES/LARGE/Z9K0091847690007.JPEG.

STAR★METHODS

KEY RESOURCES TABLE

REAGENT or RESOURCE	SOURCE	IDENTIFIER
Deposited data		
Dataset	Donoghue Lab - Brown University	https://dabi.loni.usc.edu/dsi/DP2NS111817/4TM556O4G2FN
Software and algorithms		
MATLAB	MathWorks	https://la.mathworks.com/products/matlab.html
Analysis code	MATLAB	https://github.com/D-Orellana/lf-ICs-as-Internal-Neuromarkers
ICA function	Swartz Center for Computational Neuroscience	Makeig, Scott et al. "EEGLAB: ICA Toolbox for Psychophysiological Research". WWW Site, Swartz Center for Computational Neuroscience, Institute of Neural Computation, University of San Diego California <www.sccn.ucsd.edu/eeglab/>, 2000.
Violinplot function	MATLAB	Hoffmann H, 2015: violin.m - Simple violin plot using MATLAB default kernel density estimation. INRES (University of Bonn), Katzenburgweg 5, 53115 Germany. hhoffmann@uni-bonn.de https://la.mathworks.com/matlabcentral/fileexchange/45134-violin-plot
Color palette function "cbrewer2.m"	MATLAB	https://github.com/scottclowe/cbrewer2 http://colorbrewer.org/
Other		
Cerebus System	Blackrock Microsystems	https://blackrockneurotech.com/research/products/#data-acquisition-systems
Utah array	Blackrock Microsystems	https://blackrockneurotech.com/research/products/#electrodes

RESOURCE AVAILABILITY

Lead contact

Further information and requests should be directed to and will be fulfilled by the Lead Contact, Carlos Vargas-Irwin, Brown University, carlos_vargas_irwin@brown.edu.

Materials availability

The study did not generate any new materials.

Data and code availability

- Processed data from this study are available in a public repository in https://dabi.loni.usc.edu/dsi/DP2NS111817/4TM556O4G2FN.
- Raw data is available from the lead contact (carlos_vargas_irwin@brown.edu.) upon request, subject to file size for data transfer constraints.
- Analysis code for the main results is publicly available in https://github.com/D-Orellana/lf-ICs-as-Internal-Neuromarkers. Any additional data or code may be obtained from the lead contact upon request.

EXPERIMENTAL MODEL AND STUDY PARTICIPANT DETAILS

Nonhuman primate data neural activity recording

Here, using chronically implanted microelectrode arrays (Blackrock Microsystems), neural activity was recorded from 2 macaque monkeys (9–12 kg, 2–3 years of age) in the primary motor (M1), dorsal premotor (PMd), and ventral premotor (PMv) regions. All animal handling procedures were approved by the Association for Assessment and Accreditation of Laboratory Animal Care, National Institutes of Health (AAALAC, NIH) and all surgeries were performed following standard sterile procedures in an approved animal surgical center. Arrays for recording M1 activity contained a grid of 48 active silicon-based microelectrodes 1 mm in length, spaced 400 um apart. The arrays were implanted in the M1 upper limb area just anterior to the central sulcus, at the level of the genu of the arcuate sulcus. The microelectrode arrays used to record PMd activity is similar to that of M1 i.e., it contained 48 microelectrodes of 1 mm in length, 400 um apart. The array for PMv recording is twice the size of the two mentioned above, this array contains 96 active silicon-based electrodes 1 mm in length and spaced 400um apart covering a

rectangular cortical region of 4 × 4 mm. These arrays were implanted in the PMv region of the upper limb, just posterior to the genu of the arcuate sulcus, at the level of the principal sulcus. Monkeys were head fixed during recording. Data acquisition and storage were performed using a Cerebus multichannel data acquisition system (Blackrock Microsystems).

METHOD DETAILS

The processing performed on the neural recordings includes blind source separation using the infomax ICA algorithm, component selection based on the location and amplitude of activity peaks, creation and analysis of activation maps based on the topographic location of electrodes and unmixing matrix weights, and evaluation of discriminative information using linear discriminant analysis (LDA). In addition, we include two processes to evaluate the potential usefulness of ICs in the development of BCI systems by implementing an algorithm for task stage detection and another for trial alignment. These processes are described in detail below.

LFP preprocessing

Preceding the blind source separation, we used power spectral estimation (PSD) to identify the frequency bands with the highest movement-related modulation during the task which are likely to be the most informative. For this purpose, we subtract the PSD obtained from a signal segment extracted 1.5s after the onset of the movement minus the PSD 1.5s before the movement. The PSD was calculated using the Welch estimation method with a 1.5-s wide Hamming window and a 10% overlap.[52,53] Figure 1 shows the results of this first analysis. In both monkeys, we identified five potentially informative frequency bands. In order not to alter the LFP signal waveform at all, the selected frequency bands were filtered using a finite impulse response filter with Hamming window and order 700.

As a second step of the LFP signal preprocessing, taking into account that the selected study bands are below 50 Hz and that we are working with a high number of channels (192 chs) sampled at 30 kHz, we subsampled the signal at 250 Hz (useful information up to 120 Hz according to Nyquist theorem), which allows us to reduce the computational load and therefore speed up the process.

Independent component analysis of LFP

To separate the different generators that compose the LFP signal, we employed independent component analysis (ICA), which has been extensively used and validated in EEG[54,55] and in LFP signals.[15,50,56,57] ICA is based on the following three presumptions (i) the data recorded by the electrode array are a spatially stable mixture of the activities of temporally independent brain sources (also noise sources), (ii) the mixture of potentials arising from different parts of the brain is linear at the electrodes, and the propagation delays from the sources to the electrodes are insignificant, and (iii) the number of sources is not greater than the number of electrodes.[58] The mathematical expression describing ICA is:

$$S(t) = W.X(t) \quad \text{(Equation 1)}$$

Where W is the initially unknown unmixing matrix, which defines the weights at which each generating source is present in the signal recorded by the sensor. Neural topographic maps of the components provide additional information about the location of the sources. The purpose of ICA is to estimate the unmixing matrix W and the N generating sources S(t), from the recorded data. There are several ICA algorithms, which differ in the estimation principle and the objective function. In this study, we use the "infomax" algorithm proposed by Bell and Sejnowski, 1995[59] and modified by Amari et al., 1996[60] and Lee et al., 1999.[61] It maximizes the joint entropy and minimizes the amount of mutual information between the components. A typical process usually applied prior to ICA is principal component analysis (PCA) to stabilize and accelerate the algorithm's convergence. However, in an initial analysis, it was observed that the prior application of PCA did not improve the quality of the extracted components. For this reason, this step was omitted.

Systematic sorting of ICs

Unlike PCA, where the identification of the most informative components is trivial, in ICA, the appropriate ordering is uncertain and the criterion for the selection of the most informative ICs depends mainly on the characteristics of the problem. A wide variety of criteria for ordering the components extracted by ICA can be found in the literature, for example, based on their variance, power, mean square error, among others.[62,63] In our case, upon visual inspection, we noted that specific ICs displayed consistent peaks in activity near known behavioral markers. Therefore, we established a method for ordering them that works as follows: First, to select specific ICs for analysis, we identified peaks that exceeded a threshold of 3.5 standard deviations. ICs with a peak count similar to the number of trials were subjected to further examination (see Figure S6 shows graphically the result of this process). Second, in each stage, for each trial and in each component, we analyze a window of 760 ms (60 ms before and 700 ms after the external marker), which includes sufficient information of the stage under analysis and avoids mixing information from multiple stages. We obtain the magnitude and inverse of the variance of the peaks\, this results in two 7x192xN_trials matrices (7 stages, 192 components, and N trials); the first one labeled *'temporal consistency'* contains the inverse of the variance of the peak locations and the second one called *'peak value'* contains the maximum values, it is important to note that since we are obtaining the inverse of the variance, the components whose activity peaks are more consistent in the time domain will be assigned a higher value in the 'temporal consistency' matrix. Next, we normalize the values of the matrices between 0 and 1 and calculate the ordering parameter by assigning a weighting of 60% to the temporal consistency and 40% to the peak amplitude employing the expression.

$$Sort\ parameter = 0.6 * 'temporal\_consistency' + 0.4 * 'peak\_value' \quad \text{(Equation 2)}$$

This procedure suggests the proper ordering of components based on temporal consistency and magnitude of activity peaks; however, there may be cases where components do not exhibit clear activity patterns, in which case a final visual inspection is necessary.

Stage detection

The algorithm for stage detection was tested using data from trials where the monkey successfully completed a trial (excluding error trials). This was done to avoid trials where the monkey might not have paid attention to the cues, or not performed the expected behavior. For the object presentation stage, we take a window of 700 ms; for the "Grip Cue" stage, the window was 1s, and for the stages from "Go" to "Reward," the window was 500 ms. The size of these windows was chosen according to the latency of the ICs, see Figure 3. Then, we detected amplitude peaks that exceeded a specific amplitude threshold, and those peaks that were within the allowed segments were marked as true positives, those that were outside were marked as false positives, windows where there should be no peaks and they were detected were marked as false negatives, and finally where there should be no peaks and the IC is effectively flat were marked as true negatives. In this way, we obtain all the parameters to calculate the accuracy and recall of the process. The value of the detection threshold was progressively increased within a loop, and in this way, we were able to plot the ROC curve of the algorithm. The optimal threshold value was selected using the geometric mean (see Figure S1).

Trial alignment

We use the Alignment Improvement Index (AI_{ix}) measure to assess whether trial alignment improves or decreases using ICs vs. external markers as a reference. To establish this metric, we start from the premise that better alignment will produce a sharper firing profile with more pronounced maxima and minima. Therefore, in a firing rate profile corresponding to a more accurate alignment, the ratio between the absolute maximum value and the mean value of the firing rate profile will be higher. In Equation 3, FR represents the temporal profile of the firing rate in a specific neuron. This profile corresponds to the spike count in a sliding window of duration T divided by T. Typical values are $T = 100ms$ or $T = 500ms$, here we use $T = 100ms$. The spike times were extracted from the raw data using the algorithm developed at.[64]

$$AI_{ix} = \frac{100 * (((abs(FR - mean(FR))) + mean(FR))}{mean(FR)} - 1 \quad \text{(Equation 3)}$$

Before evaluating the alignment, we classified the neurons into three groups: neurons with a preference for object presentation, neurons with a preference for grip instruction, and neurons with a preference for movement execution. The criterion for including neurons in any of these groups was also based on the firing rate; a threshold of 70% was chosen as the inclusion criterion. This means, for example, that if a neuron increases its firing rate by more than 70% after the presentation of the object, this neuron will be classified as a neuron with a preference for the presentation of the object. The groups are not mutually exclusive; there can be neurons with a preference for several stages simultaneously.

Analysis of spatial distribution of activation maps

By applying ICA to our database, we obtain a set of ICs formed by the linear combination of the original signals. The unmixing matrix W gives the linear combination of each IC, which assigns each channel a weight (Equation 1). To evaluate the contribution of each of the three regions studied (M1, PMd, and PMv) in the composition of the ICs, we used a Monte Carlo approach. We create a random probability distribution of the weights by shuffling (N = 10000) the elements of the matrix W, and at each shuffle, we obtain the average value of the weights in each region. This process results in N values for each electrode array representing each region's average randomized IC weight distribution. With these N values, we create the random probability distribution curves shown in Figure 5A and obtain the confidence limits of $\pm 99\%$. To estimate the contribution of each region, we compare the actual mean value of the weights of each region with the confidence limits obtaining three levels of activity, more than expected by chance, less than expected by chance, and within the range of expected by chance (Figures 5B and 5C).

Decoding of object and grip types

To evaluate the amount of useful discriminant information in planning and execution stages, we divided the task into two segments, the first one from object presentation to the GO signal and the second one from hand contact with the object until 3 s later. Besides allowing us to evaluate the information in planning and execution independently, this method allows us to attenuate the differences in reaction time between one trial and another. The classification was performed using Linear Discriminant Analysis (LDA) trained with 70% of the data and tested with the remaining 30%. Features were extracted from a 50 ms sliding window with 50% overlap. The features extracted from each window correspond to the average amplitude of each IC; this results in a feature space composed of 192 elements, one value for each IC.

QUANTIFICATION AND STATISTICAL ANALYSIS

Cross-validation was used in the results presented in Figure 3 for stage detection. The dataset was divided into two equal parts: one-half was used to calculate the unmixing matrices 'W' (training set), and the other half was reserved for stage detection (testing set). This approach

reduces the risk of overfitting and provides an estimate of the model's robustness. We also examined the correlation between ICs calculated using different amounts of data to verify their stability (Figure S7).

To evaluate the contribution of the M1, PMd and PMv regions in the composition of the ICs, we used a Monte Carlo approach (Figure 5). We created a random probability distribution of the weights by shuffling (N = 10,000) elements within the weight matrix W. In each shuffle, we calculated the mean weights of each region, resulting in N values representing the random distribution of IC weights. We then used these N values to create random probability distribution curves and determine $\pm$99% confidence limits, corresponding to the null hypothesis that all areas contributed equally to each IC. Comparing the actual mean weights for each region to these confidence limits allowed us to estimate the relative contribution of each region.

To statistically evaluate the spatial correlation between ICs from the same stage (in different sessions) versus ICs from different stages (Figure 6), we performed a Kruskal-Wallis test. This is a nonparametric statistical method used to test whether a dataset comes from the same population. As a nonparametric test, the Kruskal-Wallis test does not assume normality of the data.

Regarding the results of object and grip type classification (Figure 7), the data presented include cross-validation (70% training and 30% test) with N = 100 runs. The chance probability was obtained by randomly shuffling the labels 200 times. Classification values as a function of time are presented as mean + and - one standard deviation.